January 2026

Graduation Thesis

Experimental Study on Properties of Mortar Using Laterite Sand as Fine Aggregate

Supervisor: Prof. Noriyuki Mita

Asst Prof. Bunka Son

Mie University

Faculty of Engineering

Architecture Course

422748 SENGLY SILAMONGKUL

Summary

The rapid growth of urbanization and infrastructure development in Southeast Asia has sharply increased the demand for natural river sand, which remains one of the most important fine aggregates used in mortar and concrete. However, in the Mekong River basin, particularly in Cambodia and Vietnam, excessive and often unregulated sand extraction has produced serious environmental and social consequences, including riverbank erosion, loss of aquatic habitat, land instability, and disruption of local communities. In response to these problems, stricter controls on sand mining and export have reduced the availability of natural river sand and have increased the need to identify sustainable, locally available alternative materials for construction. Within this context, laterite soil is a highly relevant candidate in Cambodia because it is abundant, inexpensive, and widely distributed. Despite this potential, its practical use as a fine aggregate in cement-based materials remains limited because of its porous structure, high water absorption, and concerns regarding reduced mechanical strength. This study was therefore conducted to evaluate whether laterite sand can be used as a partial or full replacement for natural river sand in mortar, and to clarify the conditions under which acceptable performance can be achieved.

The experimental program was designed to investigate the influence of laterite replacement ratio, water-cement ratio, and mineral admixtures on the physical and mechanical properties of mortar. To simulate the highly absorptive characteristics of Cambodian lateritic soil, Japanese Arakida soil (En-tout-cas) was used as the laterite-type fine aggregate. Natural river sand was replaced by laterite sand at five levels: 0%, 25%, 50%, 75%, and 100% by weight. In addition, three water-cement ratios, namely 0.6, 0.7, and 0.8, were selected in order to examine mortar behavior under relatively rich, intermediate, and lean paste conditions. Because porous aggregates generally increase internal voids and tend to reduce strength, two mineral admixtures were also introduced to improve the microstructure and performance of the mortar: Fly Ash (FA) and Blast Furnace Slag (BF), each used as a 15% partial replacement of cement. Based on this matrix, the study evaluated hardened density, water absorption, compressive strength, bending strength, and splitting tensile strength, with the aim of understanding not only the overall performance trends but also the mechanisms responsible for strength retention or deterioration.

The results showed that the performance of laterite mortar strongly depends on the available paste volume and the use of appropriate admixtures. In the rich mix condition with a water-cement ratio of 0.6, laterite mortar was able to maintain relatively stable performance even at high replacement levels. This indicates that when sufficient cement paste is available, the rough and angular surface texture of laterite particles can be adequately coated, allowing effective bonding with the surrounding matrix. In contrast, lean mixes with a water-cement ratio of 0.8 exhibited clear strength reduction and higher sensitivity to laterite replacement. In

these mixtures, the limited paste volume was insufficient to fully cover the larger surface area of the porous aggregate, leading to poor compaction, increased internal voids, and weaker matrix continuity. Water absorption generally increased as the laterite content increased, while hardened density showed a slight decreasing trend, both of which are consistent with the porous nature of laterite. Among all modified mixtures, the Blast Furnace Slag mixes demonstrated the most notable improvement. These specimens achieved the highest compressive strength, in some cases exceeding 50 N/mm^2, and showed a denser and more integrated internal structure. This behavior is attributed to the latent hydraulic activity of slag, which promotes additional hydration and contributes to pore refinement and matrix densification. Compared with Fly Ash, Blast Furnace Slag produced a stronger enhancement effect within the experimental conditions of this study. Furthermore, the results suggest that the rough surface morphology of laterite may also contribute positively to mechanical interlocking, helping to preserve bond performance when sufficient paste and proper mix design are provided.

Overall, this study demonstrates that laterite sand has meaningful potential as an alternative fine aggregate for mortar, but its successful use depends on careful control of mix proportions and material design. Laterite cannot simply be substituted for natural sand without considering its high absorption and porous nature. Nevertheless, when used in rich mixes and combined with suitable supplementary cementitious materials, especially Blast Furnace Slag, laterite-based mortar can achieve promising physical and mechanical performance. These findings support the possibility of reducing dependence on river sand and promoting more sustainable use of locally available materials in Cambodia. At the same time, the study indicates that further work is still necessary before broad practical implementation can be recommended. In particular, future research should include long-term durability evaluation, field-scale validation, and testing with actual Cambodian laterite sources to confirm the applicability of the present findings under real construction conditions. Even so, the results of this thesis provide a useful technical basis for the future development of environmentally responsible mortar materials using laterite as a substitute for conventional river sand.

Table of Contents

Chapter1

Introduction

1.1 Background of the Research

1.1.1 The Global Construction Context

Concrete is the foundational building block of modern human civilization. Second only to water, it is the most widely consumed substance on the planet [8]. Its unparalleled versatility, high compressive strength, durability, and cost-effectiveness have made it the indispensable material of choice for critical infrastructure, ranging from high-rise buildings and residential housing to bridges, dams, and highway networks. As global populations continue to rise and developing nations undergo rapid industrialization and urbanization, the demand for concrete production is projected to grow exponentially in the coming decades.

To fully understand the scale of resource consumption associated with this demand, one must examine the volumetric composition of a standard concrete or structural mortar mixture. Concrete is a composite material comprising a binder (usually Ordinary Portland Cement), water, and aggregates. While the cement paste acts as the chemical glue that binds the matrix together, the aggregates act as the structural skeleton of the composite, providing volume stability and significantly reducing the shrinkage and heat generation that would occur if pure cement paste were used alone [8].

Aggregates are generally classified into coarse aggregates (gravel or crushed stone) and fine aggregates (sand). In a typical concrete mixture, fine aggregates account for approximately 30% to 40% of the total volume [8]. The primary role of the fine aggregate is to fill the interstitial voids between the larger coarse aggregate particles, thereby ensuring a dense, cohesive, and workable fresh mix. Historically, natural river sand has been the absolute preferred choice for this role. River sand is naturally graded over centuries by water currents, resulting in hard, chemically inert, and smoothly rounded silica particles that provide excellent workability without demanding excessive mixing water.

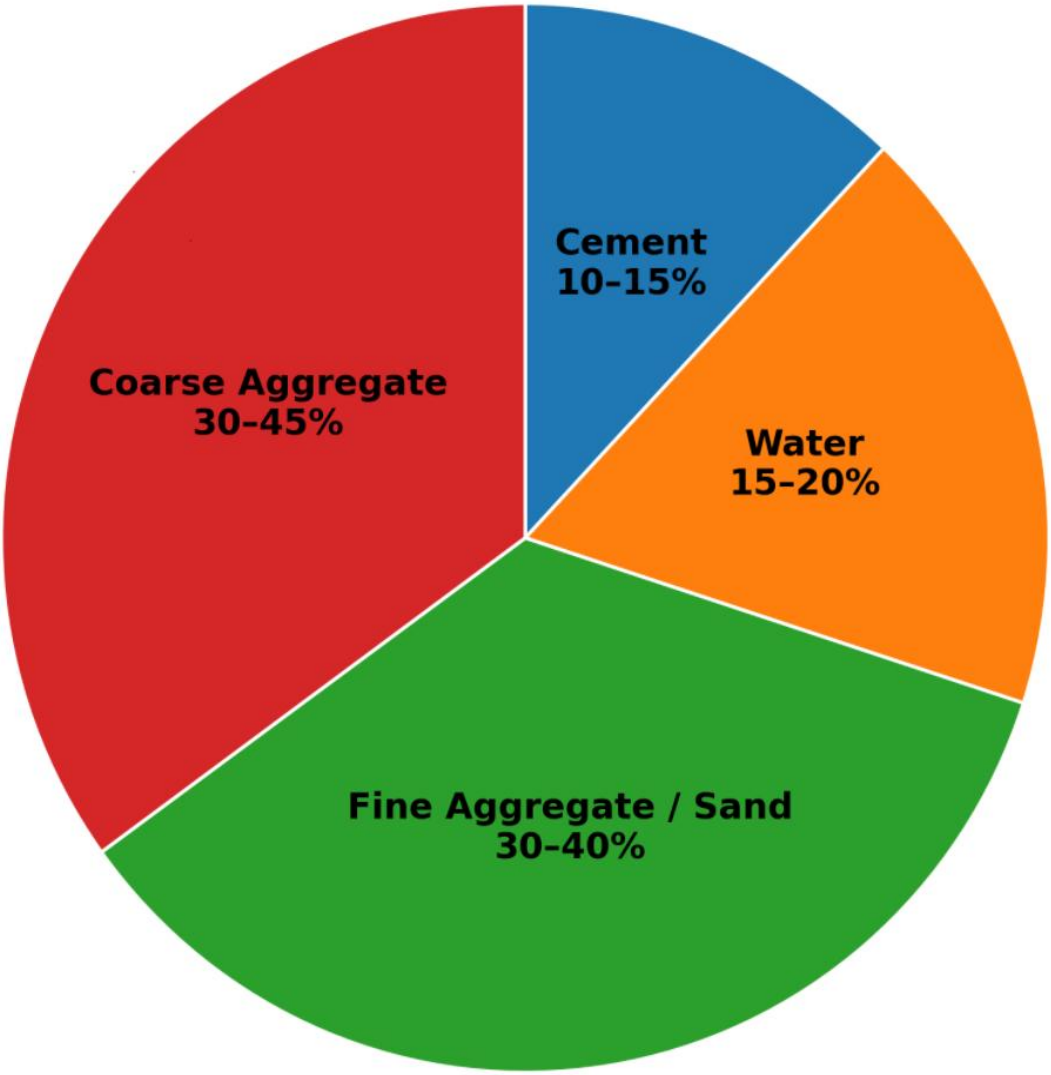

Fig 1.1: Typical Volumetric Composition of Standard Concrete

Because fine aggregate constitutes such a massive volumetric fraction of the final product, the global dependency on river sand has reached staggering figures. According to reports by the United Nations Environment Programme (UNEP), global sand and gravel consumption exceeds 40 to 50 billion metric tons annually. This relentless pace of extraction sets the stage for a severe environmental and economic crisis, as the consumption of natural sand currently vastly outstrips the natural geological rates of weathering and river replenishment. [1]

1.1.2 The Sand Crisis in Southeast Asia

Nowhere is this global dependency on natural aggregates more visible than in Southeast Asia. Over the past two decades, countries such as Cambodia and Vietnam have experienced a massive construction boom. Rapid economic growth, industrialization, and foreign direct investment have fueled the continuous development of mega-infrastructure projects, including highways, bridges, dams, and expansive urban high-rise developments in cities like Phnom Penh, Sihanoukville, and Ho Chi Minh City. This unprecedented wave of construction requires millions of cubic meters of concrete, which in turn demands an astronomical volume of high-quality river sand [9].

1.1.3 Environmental Impact on the Mekong River

Beyond the economic strain, the most alarming consequence of this aggregate demand is the devastating environmental impact on the Mekong River. The Mekong is a vital transboundary river system that supports the livelihoods, agriculture, and biodiversity of millions of people. Unregulated and intensive sand mining operations directly alter the hydrodynamics and geomorphology of the riverbed [12]. By continuously removing vast quantities of sediment, dredging vessels induce 'riverbed incision'—a phenomenon where the river channel becomes artificially deep and unnaturally steep.

This morphological alteration triggers a cascade of ecological disasters. First, the steepening of the riverbed undermines the structural integrity of the riverbanks. Without the natural slope of sediment to support them, riverbanks become highly susceptible to sudden and catastrophic collapse. In recent years, numerous incidents have been recorded along the Mekong where entire stretches of agricultural land, rural roadways, and riverside houses have plummeted into the river, displacing communities and causing tragic loss of life[12].

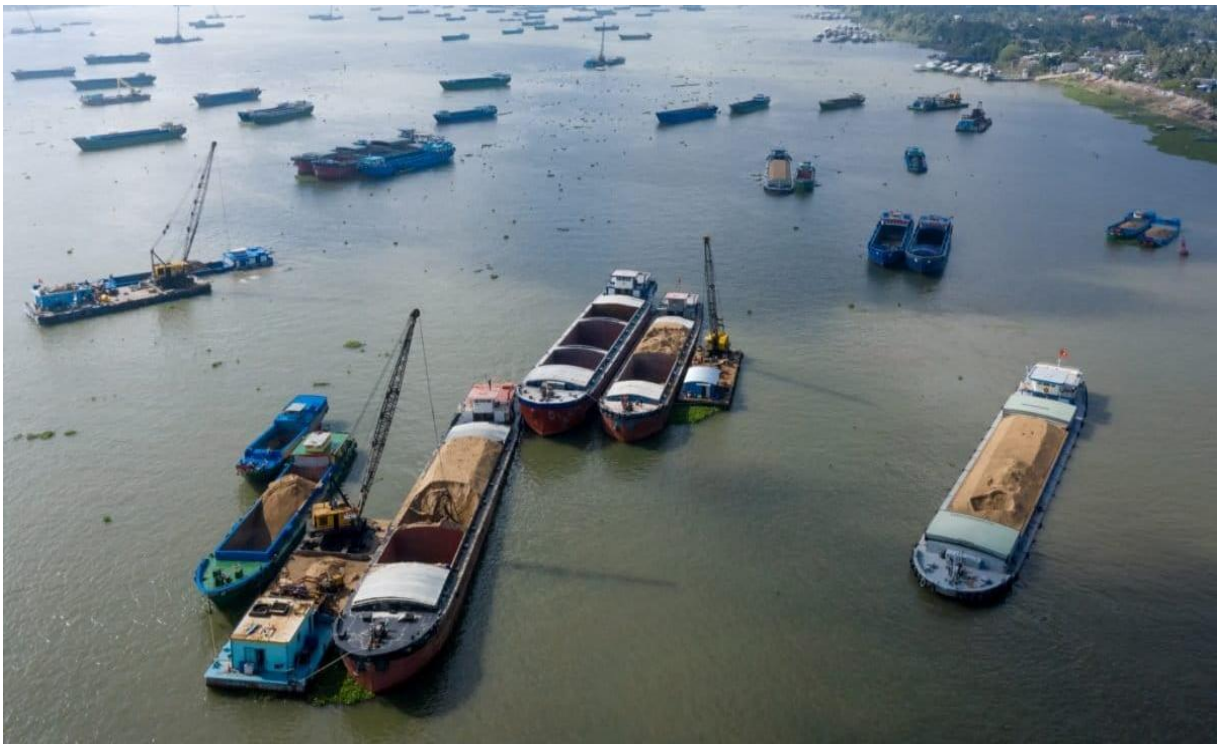

Fig 1.2: Environmental Impact of Sand Mining on the Mekong River

Second, the deepening of the river channel has exacerbated the severe issue of saline intrusion[12]. During the dry season, the lower elevation of the riverbed allows saltwater from the South China Sea to travel significantly further upstream into the Mekong Delta. This saltwater contaminates freshwater aquifers and destroys rice paddies, posing a direct threat to regional food security. Third, the mechanical churning of the dredging process increases water turbidity and destroys the benthic habitats essential for fish spawning, leading to a drastic reduction in local fish populations.

Recognizing these catastrophic environmental risks, regional governments have been forced to intervene. For example, Cambodia, which was historically a massive exporter of river sand to countries like Singapore for land reclamation, implemented strict export bans in 2017 to protect its ecosystems [2]. While such regulatory measures are vital for ecological preservation, they have further restricted the supply of sand for domestic use. Consequently, the construction industry is now at a critical juncture: to maintain infrastructure development

without destroying the environment, it is imperative to identify, validate, and adopt sustainable, locally available alternative materials.

1.2 Focus Material: Laterite Soil

1.2.1 Geological Origin and Characteristics

To address the dual challenges of the river sand shortage and the environmental degradation of the Mekong River, this study turns to a naturally abundant local resource: Laterite soil. Laterite is a soil type uniquely formed in hot and wet tropical or subtropical regions, making it a prominent geological feature in Southeast Asian countries like Cambodia. The formation of laterite is driven by a prolonged and intensive weathering process known as 'laterization.' During this process, heavy tropical rainfall continuously leaches away soluble minerals from the parent bedrock—such as silica, calcium, sodium, and magnesium—leaving behind a residual concentration of highly insoluble elements [3].

The remaining soil matrix becomes heavily enriched in iron oxides (such as hematite and goethite) and aluminum oxides. It is this high concentration of oxidized iron that imparts the characteristic rusty-red or reddish-brown coloration to laterite soils. From a microstructural perspective, this leaching process leaves behind a highly vesicular and porous structure. Unlike natural river sand, which consists of solid, dense, and rounded quartz grains, laterite particles are irregular, angular, and riddled with microscopic voids. This inherent porosity fundamentally alters the material's physical behavior, particularly its interaction with moisture, resulting in an exceptionally high water absorption capacity [3].

1.2.2 Current Utilization and Limitations

Historically, Laterite has been a material of immense cultural and architectural significance in Cambodia. Because laterite soil is relatively soft when moist and freshly excavated from the ground, it can be easily cut into large, uniform blocks. Upon prolonged exposure to air and sunlight, the iron and aluminum oxides dehydrate and crystallize, causing the blocks to harden significantly. The ancient Khmer Empire masterfully utilized this property;

laterite blocks form the hidden structural foundations, core retaining walls, and extensive enclosure perimeters of the world-renowned Angkor Wat temple complex and other monuments scattered throughout the region.

In contemporary Cambodia, laterite is still heavily utilized, but primarily in low-value civil engineering applications. It is the dominant material used for the construction of rural, unpaved 'red dirt' roads, and is frequently used as a cheap sub-base fill material for highway construction or basic landscaping. However, despite its massive abundance and low extraction cost, it is almost universally rejected by modern engineers as a fine aggregate for structural concrete or mortar.

Fig 1.3: Traditional and Modern Utilization of Laterite in Cambodia

The reluctance to utilize laterite in modern cementitious composites stems from its physical limitations. In standard concrete mix design, aggregates are expected to be hard, dense, and possess low water absorption to ensure optimal strength and workability. Laterite's high porosity means it acts like a sponge; if introduced dry into a concrete mixer, it will rapidly absorb the mixing water intended for cement hydration, resulting in a severe loss of workability (slump loss) and making the concrete difficult to pour and compact. Furthermore, the lower specific gravity and lower crushing value of the porous laterite particles lead to the assumption

that the aggregate will act as the 'weak link' in the concrete matrix, inevitably causing a drastic reduction in compressive strength. As a result, standard building codes and practices largely exclude laterite from structural applications, leaving this vast resource largely untapped.

1.3 Problem Statement

The construction industry in Southeast Asia is caught in a critical dilemma. On one hand, infrastructure development must continue to support economic growth; on the other hand, the continuous mining of river sand from the Mekong River is causing irreversible ecological damage. The reliance on river sand must be drastically reduced. Fortunately, countries like Cambodia possess millions of tons of laterite soil, which is currently excavated cheaply but utilized only for low-tier applications such as dirt roads.

The primary barrier preventing the utilization of laterite in structural mortar and concrete is a critical knowledge gap. Because laterite is highly porous, lightweight, and contains a large fraction of fine particles, it fundamentally alters the rheology and hydration dynamics of cementitious mixtures. Without empirical data and established mix-design guidelines, engineers and contractors cannot safely adopt it. There is an urgent need for rigorous scientific proof to determine how much river sand can be safely replaced by laterite, how the water-cement ratio must be adjusted to handle its high absorption, and whether the inherent weaknesses of porous aggregates can be mitigated using modern mineral admixtures. Providing this scientific validation is the core problem this thesis seeks to address.

1.4 Objectives of the Study

The overarching goal of this research is to evaluate the feasibility of utilizing porous Laterite Sand as a sustainable, eco-friendly replacement for natural river sand in mortar. To achieve this, the study aims to establish the mechanical limits of the material and explore methods for microstructural enhancement. The specific objectives are as follows:

- **1. Evaluate the Feasibility of Sand Replacement:** To investigate the physical and mechanical effects of replacing standard river sand with Laterite Sand at varying ratios (0%,

25%, 50%, 75%, and 100%). The study will quantify the impact of the aggregate's rough surface texture and porosity on compressive, bending, and splitting tensile strengths.

- **2. Optimize the Water-Cement Ratio (W/C):** To identify the operational limits of the cement paste volume when interacting with high-fines laterite. By testing rich (W/C 0.6), standard (W/C 0.7), and lean (W/C 0.8) mixtures, the study aims to determine the threshold at which the mortar fails due to insufficient paste coverage.
- **3. Investigate the Synergistic Effects of Admixtures:** To determine if the addition of supplementary cementitious materials can overcome the strength deficits caused by porous aggregates. Specifically, the study compares the effectiveness of replacing 15% of the cement with Fly Ash (FA) versus Blast Furnace Slag (BF) in 100% laterite mixtures, analyzing their ability to densify the Interfacial Transition Zone (ITZ).

Chapter 2
Theoretical Background

To accurately interpret the experimental results of this study, it is essential to establish a strong theoretical foundation regarding the chemical and physical behaviors of the materials involved. This chapter explores the underlying mechanisms of cement hydration, the microstructural effects of porous aggregates, and the chemical synergy introduced by supplementary cementitious materials.

2.1 Mechanism of Cement Hydration

Ordinary Portland Cement (OPC) is a complex blend of inorganic compounds, primarily consisting of calcium silicates. When OPC is mixed with water, it does not merely dry out; rather, it undergoes a series of irreversible, exothermic chemical reactions known collectively as hydration [4,8].This process transforms the fluid cement paste into a rigid, rock-like binding matrix.

The two most critical compounds in OPC responsible for strength development are tricalcium silicate (often denoted as C3S in cement chemistry notation) and dicalcium silicate (C2S). Upon the introduction of water, these anhydrous phases rapidly dissolve and precipitate, resulting in two primary hydration products: Calcium Silicate Hydrate (C-S-H) gel and Calcium Hydroxide (Ca(OH)2), also known as portlandite [4].

1. Calcium Silicate Hydrate (C-S-H) Gel: The C-S-H gel is the most abundant reaction product, making up approximately 50% to 60% of the volume of the fully hydrated cement paste [8]. Structurally, it is a rigid, amorphous (non-crystalline) nano-porous gel that grows outward from the cement grains. This gel acts as the primary 'glue' or binder of the concrete. It extends into the surrounding space, enveloping and interlocking with the fine and coarse aggregate particles, thereby giving the concrete its compressive strength and solid structure.

2. Calcium Hydroxide (CH): Calcium Hydroxide is formed as a crystalline byproduct of the hydration of C3S and C2S, occupying about 20% to 25% of the paste volume. Unlike the C-S-H gel, CH crystals do not contribute significantly to the mechanical strength of the concrete. In fact, because CH is relatively soluble in water and structurally weak, large deposits of CH—particularly at the boundaries between the cement paste and the aggregates—can act as weak planes where micro-cracks initiate under stress.

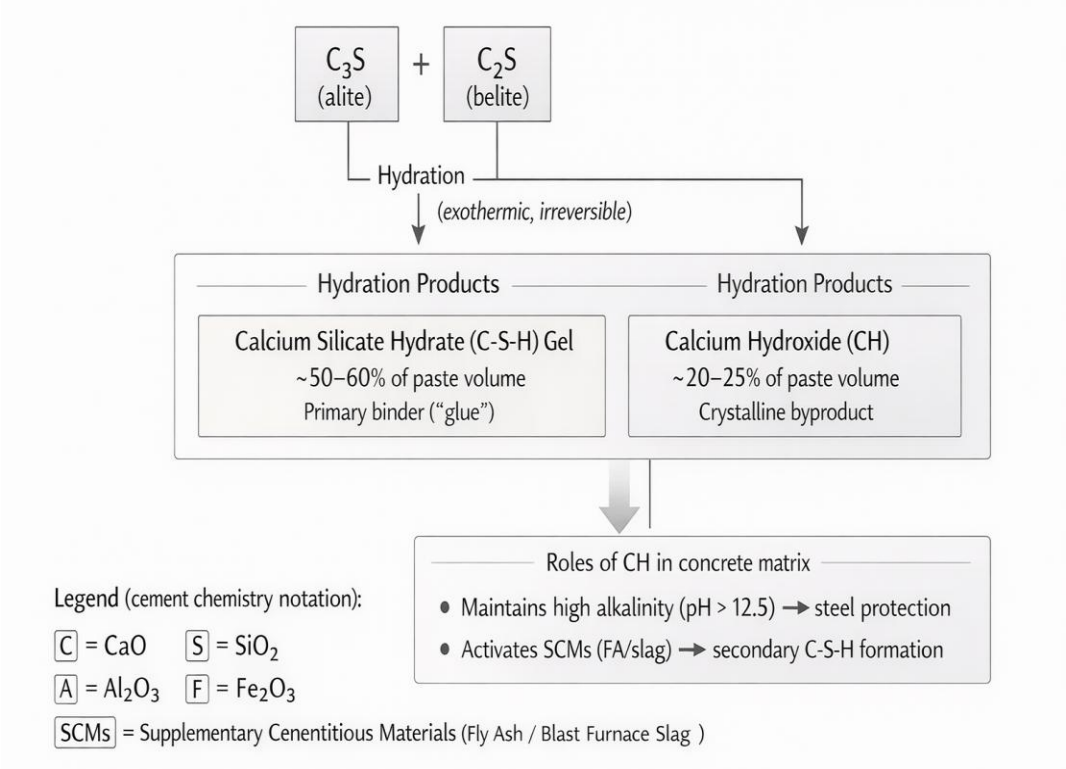

Fig 2.1: Chemical Process of Cement Hydration

However, the presence of Calcium Hydroxide is not entirely detrimental. It plays two vital roles in the lifespan of the concrete matrix. First, it maintains a highly alkaline environment (pH > 12.5) within the pore solution, which protects internal steel reinforcement from corrosion [8]. Second, and most importantly for this study, Calcium Hydroxide serves as the essential chemical catalyst required to activate Supplementary Cementitious Materials (SCMs). Without the CH byproduct generated during this initial hydration phase, admixtures such as Fly Ash and Blast Furnace Slag would remain largely inert. Understanding this chemical dependency is critical to explaining the strength recovery observed when these admixtures are added to Laterite mortar.

2.2 Theory of Porous Aggregates

In conventional concrete design, fine aggregates are largely treated as inert, non-reactive filler materials that merely occupy space and provide volume stability. However, when transitioning from standard river sand to a lateritic aggregate, the physical properties of the

aggregate itself become a highly active variable in the mixture. Understanding the theory behind porous aggregates is essential to predicting the behavior of the fresh and hardened mortar.

2.2.1 Mechanical Interlocking and the ITZ

In any concrete or mortar composite, the strength of the material is not solely determined by the strength of the cement paste or the strength of the aggregate. Instead, failure typically originates at the microscopic boundary where the aggregate meets the cement paste. This boundary layer is known in materials science as the Interfacial Transition Zone (ITZ) [8].

The ITZ is generally a thin layer (10 to 50 micrometers thick) surrounding the aggregate particles [8]. Due to the 'wall effect,' water tends to accumulate around the aggregate surfaces during mixing, leading to a higher local Water-Cement ratio at the boundary. As a result, the ITZ is typically characterized by high porosity and the presence of large, weak Calcium Hydroxide crystals [12] . In mixtures using natural river sand, the smooth, rounded surface of the quartz particles provides very little frictional grip. When subjected to tensile or shear stresses, the failure path easily propagates along this smooth, weak ITZ, causing the aggregate to pull out of the paste cleanly.

However, porous aggregates like Laterite fundamentally alter the mechanics of the ITZ. Crushed laterite particles possess a highly irregular, angular, and rough surface texture characterized by open surface pores and crevices. When the fresh cement paste is mixed, it physically flows into these open surface voids. As the paste undergoes hydration and hardens, it becomes physically anchored into the aggregate's topography.

This phenomenon is known as 'Mechanical Interlocking.' The interaction acts much like microscopic Velcro. Because the cement matrix is physically keyed into the rough surface of the laterite, the bond strength at the ITZ is vastly improved. Consequently, when tensile or bending forces are applied to the hardened mortar, the crack cannot easily slip around the aggregate boundary. Instead, the strong mechanical interlock forces the matrix to bear greater loads before failure, which explains why porous aggregate concretes often exhibit surprisingly resilient tensile and flexural properties despite the lower crushing strength of the aggregate itself.

2.3 Chemistry of Mineral Admixtures

To address the inherent physical weaknesses of porous aggregates like Laterite, modern concrete technology often employs Supplementary Cementitious Materials (SCMs). When standard cement paste is insufficient to create a dense matrix around highly absorptive and irregularly shaped particles, the introduction of SCMs can fundamentally alter the microstructural chemistry. In this study, Fly Ash and Blast Furnace Slag were utilized as 15% replacements for cement. While both are industrial byproducts used to improve concrete, their chemical reaction mechanisms and the speed at which they develop strength are distinctly different.

2.3.1 Pozzolanic Reaction (Fly Ash)

Fly Ash (FA) is a fine, powdery byproduct derived from the combustion of pulverized coal in thermal power plants. Physically, it consists of microscopic, solid, glassy spheres. These spherical particles provide a 'ball-bearing' effect within the fresh mortar, reducing inter-particle friction and significantly improving workability and flow. This physical characteristic is particularly useful when dealing with the high fines content and rough texture of laterite sand, which otherwise makes the mix stiff and difficult to compact.

Chemically, Fly Ash is classified as a pozzolan. A pozzolanic material is defined as a siliceous or aluminosiliceous material that, in itself, possesses little or no cementitious value [8]. It cannot harden simply by adding water. Instead, the glassy silica in the Fly Ash must undergo a secondary chemical reaction with Calcium Hydroxide (CH)—the weak crystalline byproduct generated during the primary hydration of Ordinary Portland Cement.

When moisture is present, the Fly Ash reacts with the Calcium Hydroxide to form additional, secondary Calcium Silicate Hydrate (C-S-H) gel. This process consumes the weak CH crystals and replaces them with a strong binding gel, thereby densifying the capillary pores over time. However, the critical limitation of the pozzolanic reaction is its kinetic speed. The reaction is heavily dependent on the prior breakdown of cement to supply enough Calcium Hydroxide, making it an exceptionally slow process. Consequently, Fly Ash contributes very little to early-age strength. At 7 days and even at 28 days, the fly ash particles act primarily as

inert physical fillers. Substantial strength gains from the pozzolanic reaction typically only become evident after 56 to 90 days of continuous moisture exposure.

2.3.2 Latent Hydraulic Activity (Blast Furnace Slag)

Ground Granulated Blast Furnace Slag (GGBFS) is a non-metallic byproduct of the iron manufacturing process, rapidly chilled from a molten state to form a highly reactive glassy structure. Unlike Fly Ash, Slag exhibits 'Latent Hydraulic Activity' This means that the chemical composition of slag (rich in calcium, silica, and alumina) gives it the inherent ability to react directly with water to form cementitious compounds, much like Portland cement itself [5].

However, when mixed with water alone, a protective aluminosilicate film quickly forms on the surface of the slag particles, halting further reaction. To unlock its full potential, the slag requires an alkaline activator. In a blended mortar, the highly alkaline environment (pH > 12.5) created by the hydration of Portland cement—specifically the dissolution of Calcium Hydroxide and alkalis—effectively breaks down this protective glassy film. Once activated, the slag particles undergo rapid and sustained hydration [5].

Because it reacts directly with water rather than waiting entirely on secondary byproducts, the latent hydraulic reaction of Blast Furnace Slag proceeds at a much faster rate than the pozzolanic reaction of Fly Ash. At a 15% replacement level, slag begins contributing significantly to the strength of the matrix within the first two to four weeks.

Furthermore, the synergy between Blast Furnace Slag and porous laterite aggregates is exceptional. Slag hydration demands a continuous supply of moisture to form its dense, pore-filling C-S-H gel network. As the surrounding cement paste dried, the sustained moisture environment provided by the porous laterite allowed the slag to hydrate more completely than it would in a dry, river-sand mix. The resulting proliferation of secondary C-S-H gel physically filled the micro-pores of both the cement matrix and the rough surface crevices of the laterite. This severe densification of the Interfacial Transition Zone (ITZ) effectively 'welded' the porous aggregate into the matrix, resulting in a super-dense composite with remarkably high compressive and tensile strengths [12] .

Chapter 3
Experimental Program

To validate the theoretical hypotheses discussed in the previous chapter and to determine the practical feasibility of utilizing laterite sand in structural and non-structural applications, a comprehensive experimental program was designed and executed. This chapter details the physical properties of the raw materials, the formulation of the mix proportions, the procedural intricacies of specimen preparation, and the standardized testing methodologies employed to evaluate the fresh and hardened states of the mortar.

3.1 Materials Used

The quality, origin, and physical characteristics of the constituent materials strictly govern the mechanical performance of a cementitious composite. All materials selected for this experimental program were sourced and processed in accordance with Japanese Industrial Standards (JIS) to ensure high reliability and reproducibility of the data.

3.1.1 Cement (Binder)

The primary binder utilized across all mix formulations was Ordinary Portland Cement (OPC). OPC was selected as it is the globally recognized standard for construction, allowing the results of this study to be easily extrapolated to real-world construction practices in Cambodia. The OPC used in this experiment possessed a standard density of 3.16 g/cm³. This provides the essential calcium and silica compounds necessary to form the primary load-bearing matrix.

3.1.2 Fine Aggregates: Silica Sand vs. Laterite Sand

The core variable of this experimental study is the fine aggregate. Two distinct types of fine aggregate were utilized to create a comparative baseline. The control aggregate was standard Silica Sand (River Sand), representing conventional, high-quality construction practices. The experimental aggregate was Japanese 'En-tout-cas' (Arakida-tsuchi), a crushed red clay material widely used for tennis courts, which was selected as an accurate geological simulation for Cambodian Laterite soil.

A critical and highly unusual observation regarding the physical properties of these two aggregates is their identical specific gravity. Laboratory testing confirmed that both the Silica Sand and the Laterite Sand possessed a density of exactly 1.99 g/cm³. In typical concrete research, alternative aggregates like laterite are notably lighter than quartz-based river sands. Because the densities in this study are identical, any resulting changes in the fresh unit weight or hardened density of the mortar cannot be attributed to the inherent weight of the aggregate material. Instead, variations in density must be strictly attributed to air entrapment, mixture cohesiveness, and microstructural porosity. Furthermore, while the densities are identical, the

water absorption rates differ vastly. The Silica Sand exhibited a low water absorption of 0.89%, while the highly porous Laterite Sand possessed a much higher absorption rate, fundamentally altering the fluid dynamics of the fresh paste.

Type	Properties
Cement (C)	Ordinary Portland Cement; Density: 3.16 g/cm³
Sand (S)	Silica sand; Density: 1.99 g/cm³; Water absorption: 0.89%
Laterite sand (L)	Density: 1.99 g/cm³; Water absorption: 2.38%
GGBFS (BF)	Ground granulated blast-furnace slag; Density: 2.91 g/cm³
Fly ash (FA)	Density: 2.22 g/cm³

Table 3.1: Physical Properties of Materials

Fig 3.1: Visual Comparison of Fine Aggregates

3.1.3 Particle Size Distribution (Sieve Analysis)

To further understand the physical differences between the two fine aggregates, a comprehensive sieve analysis was conducted. The gradation of an aggregate dictates the packing density of the solid skeleton and heavily influences the surface area that must be coated by the cement paste. The particle size distribution curves for both the Silica Sand and the Laterite Sand are plotted in Fig. 3.2.

The sieve analysis revealed a profound structural difference. The curve for the Laterite Sand sits noticeably higher on the finer sieve sizes (0.3 mm and 0.15 mm) compared to the Silica Sand. This indicates that the crushed Laterite contains a significantly higher percentage of fine dust, silt, and clay-sized particles. This high fines content presents a severe challenge for mix design. Fine particles possess a massive cumulative surface area. When mixed with water, these fines essentially 'drink' the available free water, dramatically increasing the water demand of the mixture. This phenomenon results in a highly cohesive, sticky, and stiff fresh mortar, necessitating careful adjustments to the Water-Cement ratio to achieve workable compaction.

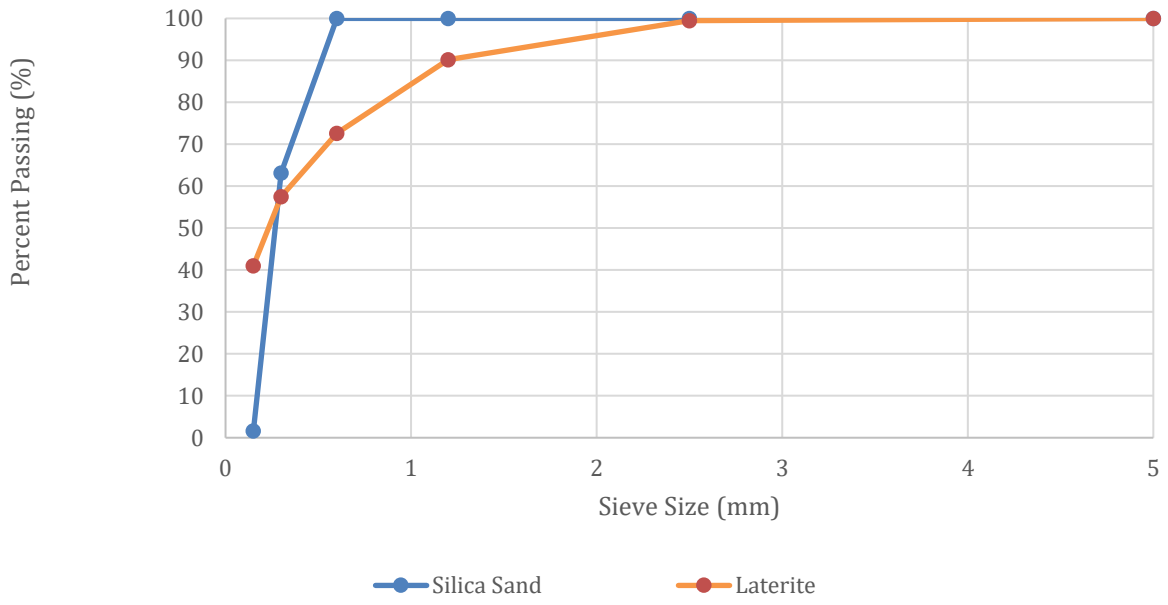

Fig 3.2: Sieve Analysis Curve (Particle Size Distribution)

3.1.4 Mineral Admixtures

Because the high porosity and high fines content of the Laterite were expected to compromise the structural integrity of the mortar, two industrial byproducts were introduced as Supplementary Cementitious Materials (SCMs) to fortify the matrix. These admixtures were used to replace 15% of the cement weight in specific experimental batches.

1. Fly Ash (FA): A Type II Fly Ash with a density of 2.22 g/cm³ was utilized. Its spherical particle morphology was intended to improve the rheology (flowability) of the sticky laterite mixture, while its pozzolanic properties were expected to slowly react with calcium hydroxide over a long-term period.

2. Blast Furnace Slag (BF): Ground Granulated Blast Furnace Slag (Type B) with a density of 2.91 g/cm³ was also tested [5]. Characterized by its rapid latent hydraulic activity, the slag requires moisture to react. It was hypothesized that the high moisture retention of the porous laterite would synergize perfectly with the slag, accelerating the formation of a dense, impermeable matrix that effectively seals the pores and enhances mechanical interlocking at the aggregate boundary.

3.2 Preliminary Trial (W/C Selection)

A fundamental challenge when utilizing highly porous aggregates like laterite is determining the appropriate Water-Cement (W/C) ratio. Because the laterite aggregate contains a high fraction of fine particles and possesses a highly absorptive surface, its water demand is vastly different from that of standard river sand. If the W/C ratio is too low, the mix will be overly stiff and impossible to compact properly, leading to large 'honeycomb' voids in the hardened state. Conversely, if the W/C ratio is too high, the mix will suffer from severe bleeding, segregation, and ultimately, poor mechanical strength [8].

To establish the optimal W/C ratios for the main experiment, a series of preliminary visual and qualitative flow trials were conducted. Rather than relying solely on the rigid parameters of the JIS R 5201 standard flow test—which was originally designed for standard

silica sands—the focus of these preliminary trials was to achieve a workable consistency that allowed for adequate placement and compaction in the molds.

The trials focused exclusively on the 100% Laterite replacement mixtures, as these represented the 'worst-case scenario' for workability. A fixed W/C ratio of 0.75 was initially selected as a starting baseline. The observations were as follows:

- Rich Mix (Aggregate-to-Cement Ratio 1:1): At a starting W/C of 0.75, the mixture was excessively fluid and exhibited severe segregation, rendering it unsuitable for casting. Through iterative adjustments, the water content was significantly reduced. A final W/C ratio of 0.60 was determined to provide the optimal cohesive paste necessary for this high-cement-content mix.
- Standard Mix (Aggregate-to-Cement Ratio 1:2): At the baseline W/C of 0.75, a rough measurement yielded a flow spread of 216 mm. While highly workable, this level of fluidity indicated an excess of free water that would likely compromise ultimate strength. The water content was therefore lowered, and an optimal W/C ratio of 0.70 was established.
- Lean Mix (Aggregate-to-Cement Ratio 1:3): At the baseline W/C of 0.75, the high volume of porous laterite absorbed a significant portion of the limited cement paste. This resulted in a stiff, dry mixture with a very low flow spread of 105–107 mm. To ensure sufficient lubrication for compaction, the water content had to be increased. A final W/C ratio of 0.80 was selected.

3.3 Mix Proportions

Based on the results of the preliminary trials, the final experimental matrix was established. The comprehensive mix proportions are detailed in Table 3.2. The experiment was divided into a 'Plain Series' (evaluating the effect of sand replacement) and an 'Admixture Series' (evaluating microstructural enhancement).

3.3.1 Replacement Methodology

A critical methodological parameter in this study is that the substitution of Silica Sand with Laterite Sand was executed strictly by weight (mass replacement). The replacement levels were systematically varied at 0%, 25%, 50%, 75%, and 100%.

In typical concrete mix design involving lightweight aggregates, replacement is often performed by volume to maintain a consistent yield. However, as established in Section 3.1, the specific gravity of the particular Laterite used in this study (1.99 g/cm³) was identical to that of the chosen Silica Sand (1.99 g/cm³). Because the densities were the same, replacing the material by weight essentially equated to replacing it by absolute volume. Therefore, any observed variations in the properties of the fresh or hardened mortar cannot be attributed to a physical mismatch in aggregate bulk volume, but rather must be analyzed through the lens of particle shape, surface texture (interlocking), and fines content.

Table 3.2: Comprehensive Mix Proportions

A/C	W/C (%)	L/A (%)	Unit Mass (kg/m³)			
			C	W	S	L
1	60	100	704	423	0	704
		75	704	423	176	528
		50	705	423	352	352
		25	705	423	528	176
		0	705	423	705	0
2	70	100	494	346	0	989
		75	494	346	247	742
		50	495	346	495	495
		25	495	346	742	247
		0	495	346	989	0
3	80	100	381	305	0	1142
		75	381	305	286	857
		50	381	305	571	571
		25	381	305	857	286
		0	381	305	1143	0

W_C	Cement_g	FA/BF_g	Water_g	Sand_g	Laterite_g	Total_binder_g	W_over_binder	C_to_SplusL	S_to_L
0.6	2240.337	395.35	1581.41	0	2635.691	2635.690909	0.6	1	100
0.7	1642.914	289.93	1352.99	0	3865.68	1932.84	0.7	2	100
0.8	1297.037	228.89	1220.74	0	4577.779	1525.926316	0.8	3	100

3.4 Specimen Preparation Process

To ensure uniformity and prevent the high-absorption laterite from disrupting the W/C ratio during mixing, strict preparation protocols were followed.

3.4.1 Mixing and Casting

All batches were mixed utilizing a standard 4-liter Hobart-type planetary mortar mixer. The mixing sequence was modified to account for the high fines content of the laterite:

1. Dry Mixing: The cement, S aggregates, and any powdered admixtures (FA or BF) were combined in the bowl and mixed at low speed for 1 minute to ensure homogenous distribution of the fine particles.

2. Wet Mixing: The predetermined amount of mixing water was added, and the mixer was operated at high speed for 3 minutes to fully activate the cement paste and coat the aggregate surfaces.

Immediately following mixing, the fresh mortar was cast into steel molds. Prism molds (40 x 40 x 160 mm) were used for bending and compressive strength testing, while cylindrical molds (φ50 x 100 mm) were prepared for splitting tensile strength evaluation. The molds were filled in two layers, with each layer systematically consolidated using a tamping rod to expel entrapped air.

3.4.2 Curing Conditions

Once cast, the specimens were covered with plastic sheeting to prevent surface moisture evaporation and left undisturbed in the molds for 24 hours. Following demolding, all specimens were fully submerged in a water curing tank maintained at a constant temperature of 20°C until their respective testing ages (1 week and 4 weeks).

The entire specimen preparation workflow, detailing the sequential steps from precise material weighing to the final water curing regime, is visually summarized in Figure 3.3. Adhering strictly to this chronological process was imperative to minimize experimental variance, particularly regarding the moisture control of the porous laterite aggregates.

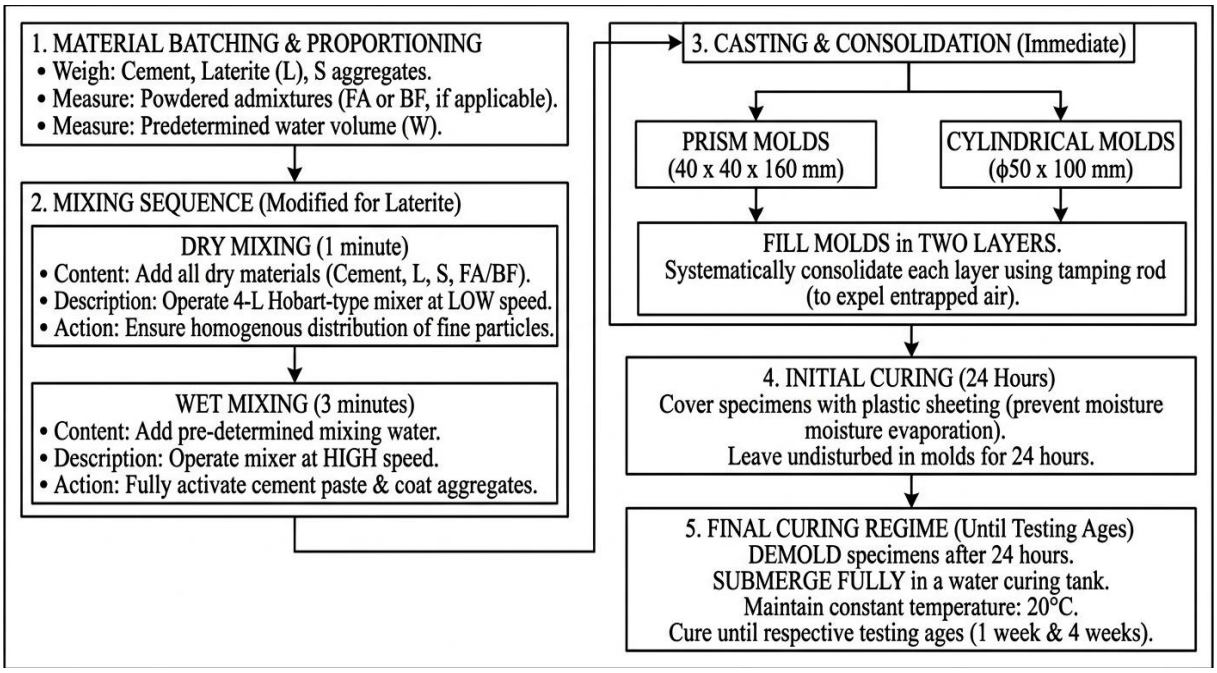

Fig 3.3: Specimen Preparation Flowchart

3.5 Testing Methods

To quantitatively evaluate the mechanical performance and physical characteristics of the hardened laterite mortar, a series of destructive and non-destructive tests were conducted at specified curing ages (1 week and 4 weeks). All testing protocols were executed in strict compliance with the Japanese Industrial Standards (JIS) to ensure the scientific validity and global comparability of the structural data obtained.

3.5.1 Bending Strength Test

The flexural capacity of the material was determined by subjecting the prismatic specimens (40 × 40 × 160 mm) to a three-point bending test. The specimen was symmetrically supported on two lower steel rollers set at a span of 100 mm. A continuously increasing concentrated load was applied to the exact mid-span of the upper face via a third roller using a Universal Testing Machine.

From a solid mechanics perspective, this loading configuration induces maximum compressive stress at the upper boundary and maximum tensile stress at the lower boundary

(the bottom soffit). Because cementitious composites are inherently much weaker in tension than in compression, fracture invariably initiates at the bottom face and propagates upward. Therefore, the bending test is an excellent indirect measure of the mortar's tensile capacity and the bond strength between the aggregate and the cement paste.

3.5.2 Compressive Strength Test (JIS A 1108)

Immediately following the bending test, the two resulting unbroken halves of the prism were utilized for compressive strength testing, adhering to the principles outlined in JIS A 1108 [6]. Each prism half was placed longitudinally between two rigid, precision-machined steel loading plates (40 × 40 mm). A uniaxial compressive force was applied steadily until the specimen suffered catastrophic structural failure (crushing).

The compressive strength (fc) was calculated by dividing the maximum recorded failure load (P) by the nominal cross-sectional area of the loading plates (A). Utilizing the broken halves of the prism is a highly efficient standard methodology, as it yields two independent compressive strength data points for every single specimen cast. This approach significantly enhances the statistical reliability of the dataset while minimizing material waste.

3.5.3 Splitting Tensile Strength Test (JIS A 1113)

While the bending test provides flexural data, it does not measure pure tension. To accurately isolate and measure the tensile capacity of the mortar, the Splitting Tensile Test (frequently referred to as the Brazilian test) was conducted in accordance with JIS A 1113 [7]. This test utilized the cylindrical specimens (φ50 × 100 mm).

In this procedure, the cylinder is placed horizontally between the platens of the testing machine. A compressive line load is applied diametrically along the entire longitudinal axis of the cylinder. According to the theory of elasticity, this specific compression geometry induces a nearly uniform tensile stress across the vertical diametrical plane. When the induced tensile stress exceeds the tensile strength of the mortar, the cylinder splits cleanly down the middle.

This test was critical for evaluating the 'Mechanical Interlocking' hypothesis of this research. By examining the fractured surface after the cylinder split, it was possible to visually determine whether the fracture path travelled around the aggregates (indicating a weak Interfacial Transition Zone) or directly through the laterite particles (indicating a superior mechanical bond).

3.5.4 Physical Properties (Density and Water Absorption)

Beyond mechanical strength, the durability and microstructural density of the mortar were evaluated through water absorption and hardened density testing at the 7- and 28-day marks. The procedure involved a rigorous moisture-conditioning cycle designed to isolate the volume of the capillary pores and accurately determine the relevant physical metrics.

To accommodate the testing schedule, the conditioning process was initiated 24 hours prior to each target age—specifically on the 6th and 27th days. At these intervals, the specimens were removed from their curing environment, wiped to a Saturated Surface Dry (SSD) condition, and their SSD mass was recorded. Subsequently, the specimens were placed in a ventilated drying oven at 105°C for 24 hours. Following this drying period, which aligned exactly with the 7-day and 28-day testing milestones, the specimens were removed and their Absolute Dry Mass was measured.This systematic procedure yielded all the necessary mass data—both the SSD and oven-dry weights—required to concurrently calculate both the water absorption and the hardened density. The difference between the SSD mass and the Absolute Dry Mass directly quantifies the volume of permeable voids within the matrix. The Hardened Density was then calculated by dividing the Absolute Dry Mass by the geometrically determined volume of the specimen. These physical metrics served as the primary basis for the correlation analysis discussed in Chapter 5.

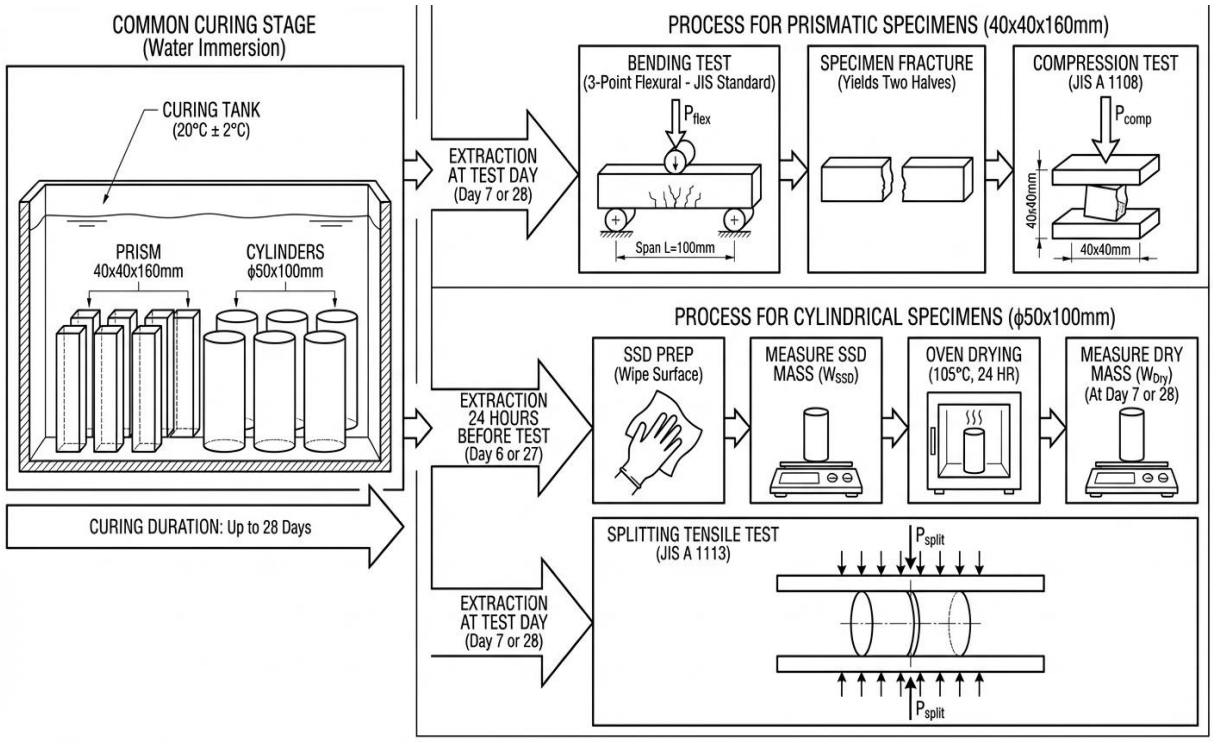

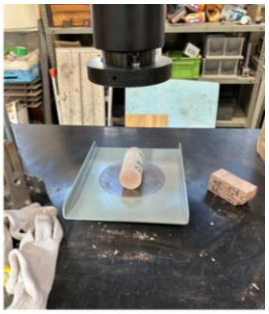

BENDING SPLITTING

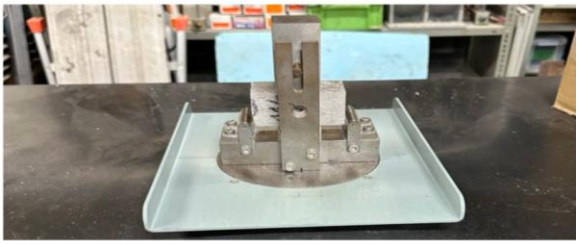

COMPRESING

Fig 3.4: Testing Setup

Chapter 4
Experimental Results

This chapter presents the empirical data obtained from the comprehensive testing program outlined in Chapter 3. The results are systematically categorized into physical properties and mechanical strength characteristics. The objective is to analyze the behavioral trends of the mortar as the replacement ratio of natural river sand with laterite sand increases from 0% to 100%, across various Water-Cement (W/C) ratios.

4.1 Hardened Physical Properties

The physical properties of hardened mortar, specifically density and water absorption, are fundamental indicators of the composite's microstructural integrity. Analyzing these parameters provides essential context for understanding the ultimate mechanical failure mechanisms observed in the compression and tensile tests.

4.1.1 Hardened Density Analysis

A consistent, albeit slight, decreasing trend in bulk density was observed as the proportion of Laterite sand increased. For example, in the W/C 0.6 series, the density decreased marginally from the control baseline to the 100% replacement level. In conventional concrete research, a drop in density upon the introduction of a new aggregate is typically assumed to be a direct consequence of the new aggregate possessing a lower specific gravity than the original material [8].

However, as meticulously documented in the materials characterization phase (Chapter 3, Table 3.1), the specific gravity of the Laterite sand used in this experiment (1.99 g/cm³) was verified to be strictly identical to that of the control Silica Sand (1.99 g/cm³). Because the absolute mass of the solid materials did not change, the observed reduction in the final hardened density cannot be attributed to the aggregate's innate weight.

Instead, this density reduction is a direct consequence of altered fresh state rheology leading to variations in compaction. As demonstrated by the sieve analysis, the Laterite sand contained a vastly higher proportion of fine particles (silt and clay fractions) than the clean river sand. This high fines content drastically increased the water demand of the mixture, resulting in a fresh mortar that was highly cohesive, viscous, and 'sticky.' During the casting phase, this increased viscosity hindered the natural expulsion of entrapped air bubbles, despite standard tamping procedures. Consequently, a slightly higher volume of macroscopic air voids was locked into the laterite mixtures, which mathematically lowered the overall bulk density of the hardened composite.

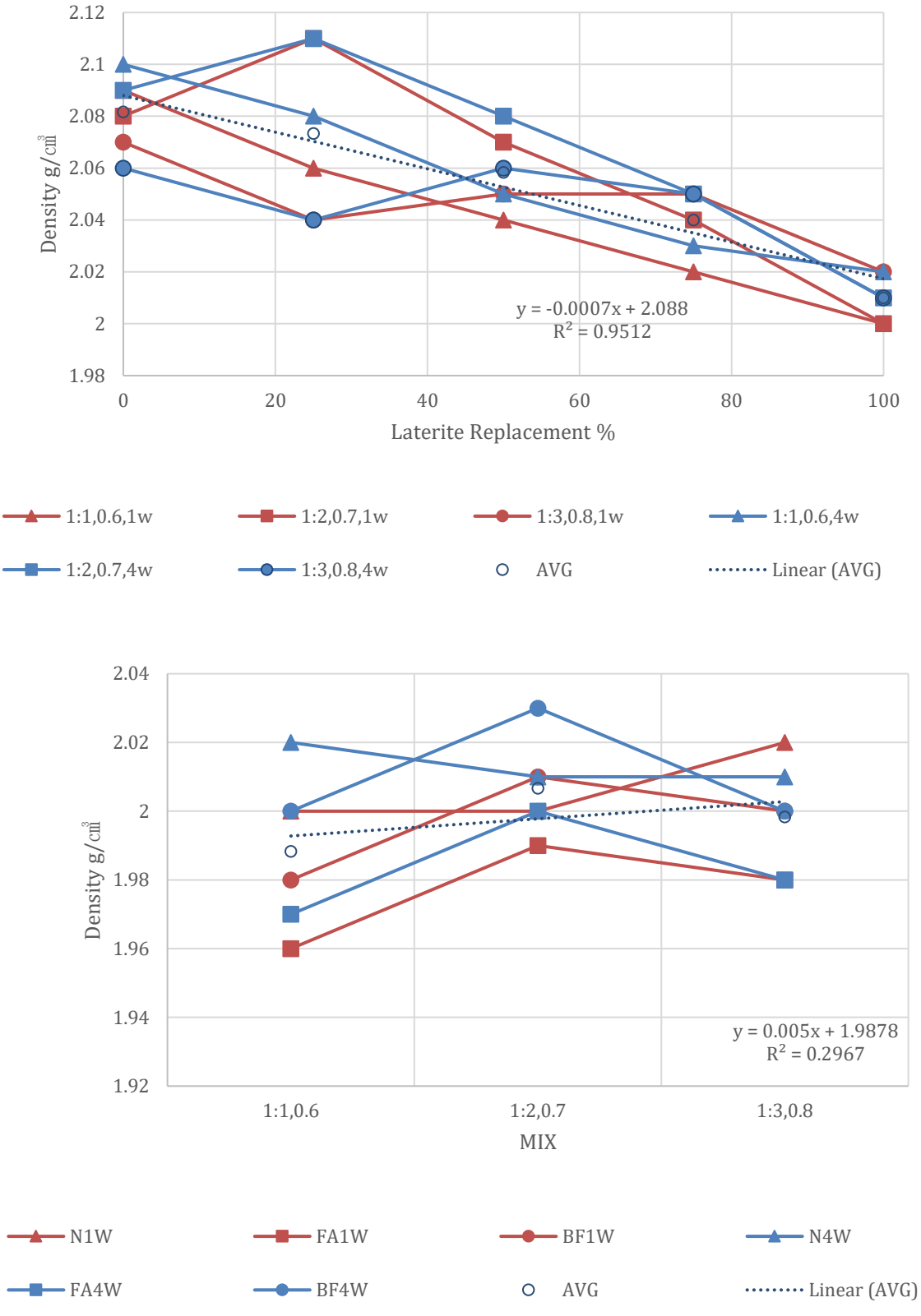

Fig 4.1: Relationship between Laterite Replacement Ratio and Hardened Density

4.1.2 Water Absorption Characteristics

Water absorption testing serves as an indirect measure of the permeable void space (capillary porosity) within the hardened cementitious matrix. Generally, incorporating a highly porous aggregate into a concrete mix is expected to elevate the total water absorption of the final product, as the aggregate itself provides a pathway for water ingress. However, the experimental data plotted in Figure 4.2 reveals a highly counter-intuitive phenomenon.

Contrary to standard expectations, the total water absorption of the mortar matrix actually exhibited a decreasing trend as the Laterite replacement ratio increased. The specimens containing 100% Laterite sand consistently absorbed less water than the 0% control specimens composed entirely of standard river sand.

This unexpected reduction in permeability is scientifically attributed to the 'Filler Effect' generated by the micro-fines inherent to the crushed laterite. While the parent laterite aggregate particles are indeed porous, the mechanical crushing process generates a substantial volume of microscopic dust. During the wet mixing phase, these ultra-fine particles disperse uniformly throughout the cement paste. As the paste hardens, these fines act as micro-plugs, physically occupying and blocking the interconnected capillary channels that typically form as excess mixing water evaporates.

By filling these microscopic voids, the laterite fines significantly increase the 'tortuosity' of the pore network—meaning water attempting to penetrate the matrix is forced to take a highly convoluted and obstructed path. Therefore, even though the overall bulk density decreased slightly due to entrapped macro-air bubbles (as discussed in Section 4.1.1), the continuous capillary network was heavily disrupted by the Filler Effect, ultimately resulting in a more watertight and less absorptive composite material.

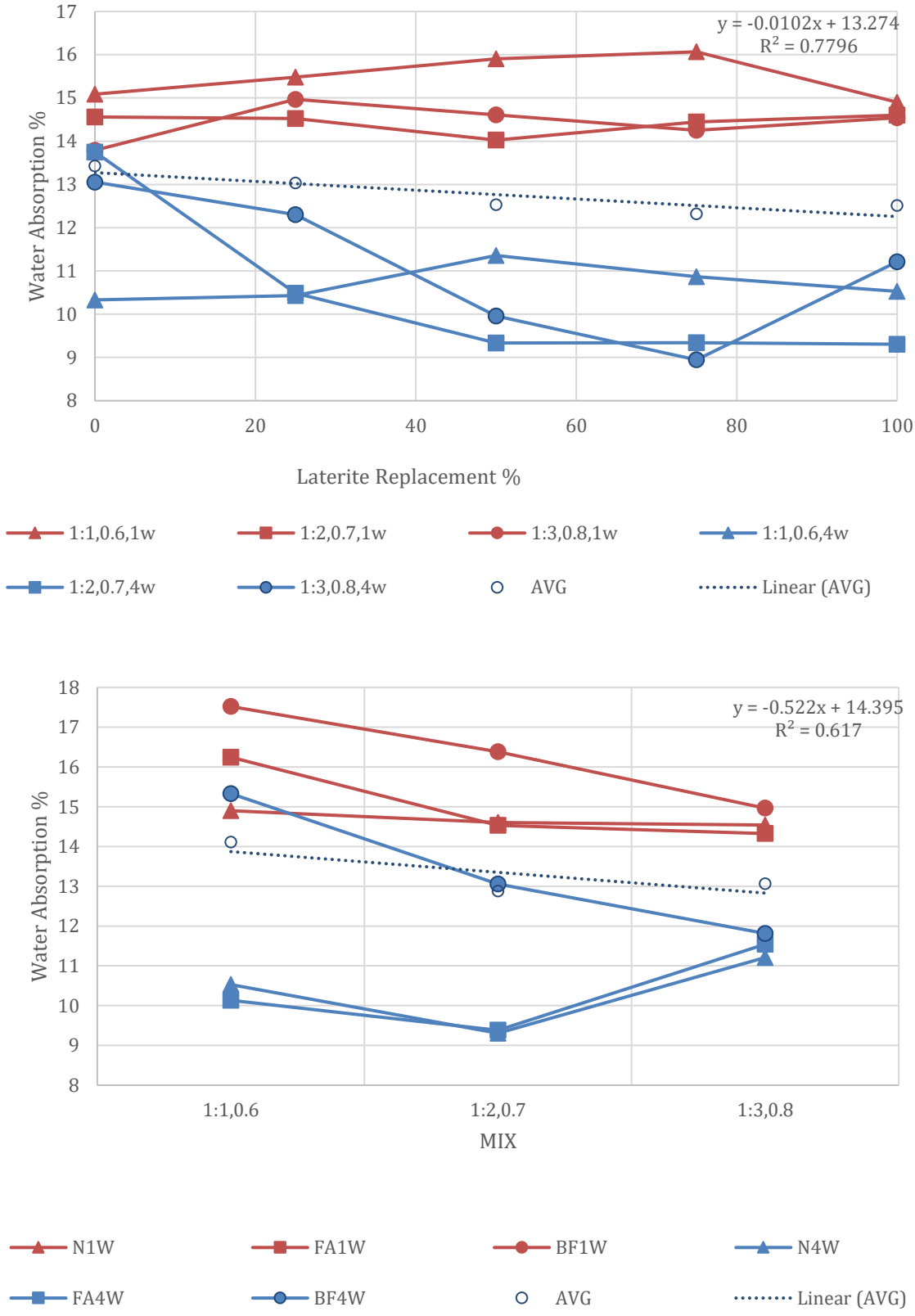

Fig 4.2: Relationship between Laterite Replacement Ratio and Water Absorption

4.2 Compressive Strength of Plain Mixes

Compressive strength is universally recognized as the most critical parameter for evaluating the structural viability of cementitious composites. In this study, the 28-day compressive strength of the plain mortar mixes (without admixtures) was evaluated across various Laterite replacement ratios and Water-Cement (W/C) ratios. Figure 4.3 illustrates the resultant mechanical behavior, which reveals a highly divergent performance dependent on the initial cement paste volume.

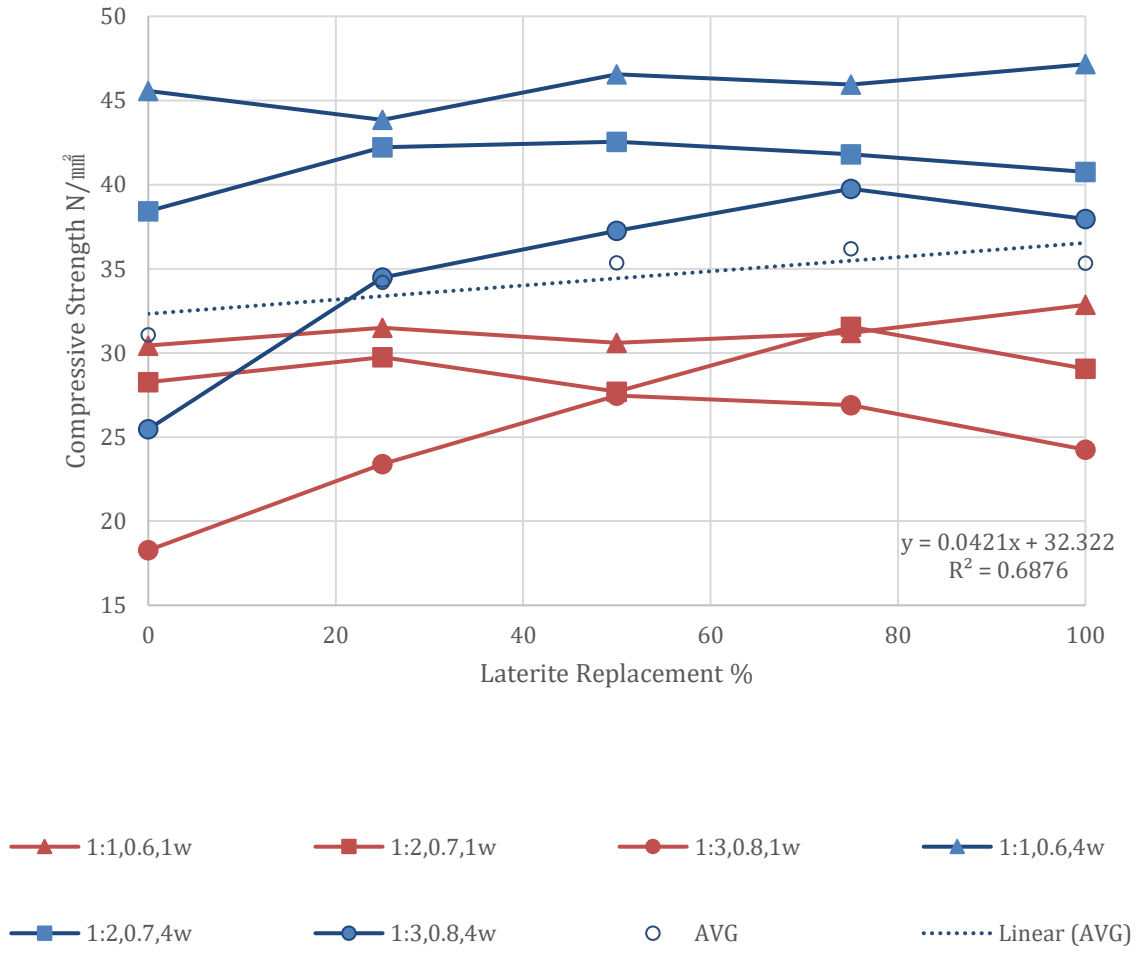

Fig 4.3: Compressive Strength vs. Laterite Replacement Ratio

4.2.1 Stability of Rich Mixes (W/C 0.6)

A remarkable observation from the experimental data is the structural resilience of the 'Rich Mixes' (W/C 0.6 with an Aggregate-to-Cement ratio of 1:1). Conventional material science dictates that substituting a hard, non-porous aggregate (river sand) with a weaker, highly porous aggregate (crushed laterite) should induce a corresponding loss in overall compressive strength [8]. However, the data reveals that the strength remained exceptionally stable, fluctuating narrowly between 32.8 N/mm² (0% Laterite) and 30.4 N/mm² (100% Laterite).

This retention of strength is scientifically attributed to two primary mechanisms: the 'Filler Effect' and superior 'Mechanical Interlocking.' First, the high volume of fine particles within the laterite effectively filled the microscopic voids in the matrix, creating a denser paste structure. Second, unlike the smooth, water-worn surface of river sand, the crushed laterite particles possess a highly angular, irregular, and rough surface texture. Because the W/C 0.6 mixture contained an abundance of cement paste, the binder was able to fully coat these irregular aggregates. The hardened cement paste securely anchored itself into the rough surface crevices of the laterite, creating a profound mechanical grip at the Interfacial Transition Zone (ITZ). This intense interlocking effectively neutralized the innate weakness of the porous aggregate, allowing the composite to resist high crushing loads.

4.2.2 Failure Mechanism of Lean Mixes (W/C 0.8)

In stark contrast to the rich mixes, the 'Lean Mixes' (W/C 0.8 with an Aggregate-to-Cement ratio of 1:3) experienced a catastrophic decline in compressive strength. As the laterite replacement ratio escalated to 100%, the strength plummeted from 24.2 N/mm² to 18.2 N/mm².

This degradation is best explained by the 'Paste Volume Theory.' As demonstrated by the sieve analysis, the laterite sand contains a significantly higher fraction of fine dust compared to river sand. This high fines content exponentially increases the specific surface area of the total aggregate skeleton. In a lean mix, the absolute volume of cement paste is fundamentally limited. When 100% laterite is utilized, there is simply not enough cementitious 'glue' to thoroughly coat the vast surface area of the porous particles and fill the inter-granular voids.

Consequently, the mixture becomes starved of paste. The Interfacial Transition Zone (ITZ) forms weakly, with numerous dry contact points between raw aggregate particles. Under compressive loading, these poorly bonded interfaces act as structural stress concentrators, initiating premature micro-cracking and leading to early macroscopic failure. This establishes a strict limit on the utilization of laterite: it cannot be used safely in lean, low-cement masonry formulations without severe strength penalties.

4.3 Effect of Mineral Admixtures on Compressive Strength

To overcome the microstructural weaknesses associated with 100% laterite replacement—particularly in higher W/C ratios—the efficacy of Supplementary Cementitious Materials (SCMs) was investigated. In this phase, 15% of the cement mass was replaced by either Fly Ash (FA) or Ground Granulated Blast Furnace Slag (BF). The comparative compressive strength results at 28 days are presented in Figure 4.4.

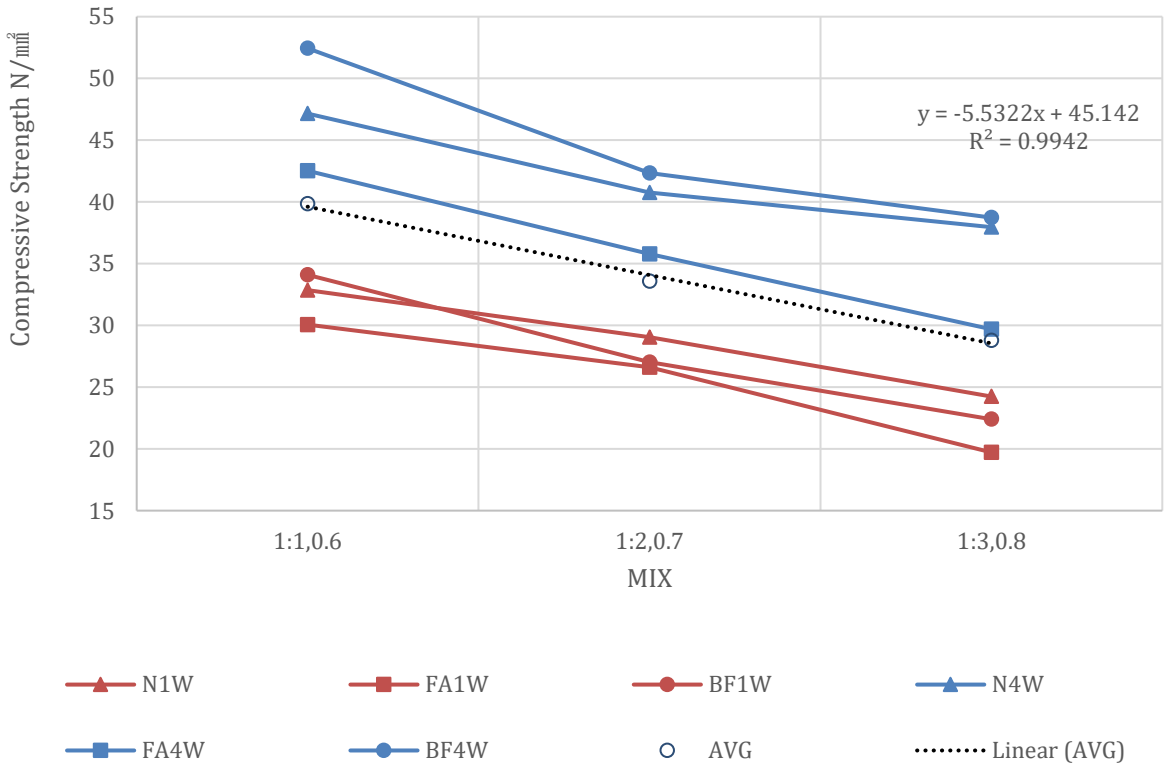

Fig 4.4: Effect of Admixtures on Compressive Strength (100% Laterite)

The experimental data reveals a massive divergence in performance between the two admixtures. The introduction of Blast Furnace Slag (BF) yielded an extraordinary enhancement in load-bearing capacity. For the W/C 0.6 configuration, the compressive strength skyrocketed to 53.9 N/mm², representing a drastic improvement over the 30.4 N/mm² achieved by the Plain 100% laterite mix. Even in the highly challenging lean mix (W/C 0.8), the BF slag managed to recover the structural deficit, pushing the strength back up to 38.7 N/mm².

This remarkable success is rooted in the Latent Hydraulic Activity of the slag. When activated by the high alkalinity of the Portland cement, the fine slag particles react aggressively to form a secondary generation of Calcium Silicate Hydrate (C-S-H) gel. This newly formed gel precipitates directly into the capillary pore spaces and, most importantly, into the micro-crevices of the porous laterite aggregate. This chemical reaction profoundly densifies the Interfacial Transition Zone (ITZ), transforming the boundary layer from a weak slip-plane into a rigid, unified matrix. The slag effectively 'welds' the porous aggregate into the concrete structure [12] .

Conversely, the Fly Ash (FA) mixtures demonstrated negligible to minor improvements at the 28-day mark, generally matching or slightly underperforming the Plain mixes (e.g., yielding 30.0 N/mm² at W/C 0.6). Because the pozzolanic reaction of Fly Ash is chemically delayed, requiring the slow breakdown of Calcium Hydroxide, it acted primarily as an inert physical filler during the first four weeks of curing. While it may provide long-term durability benefits beyond 90 days, it is not an effective solution for achieving early structural strength in laterite-based composites.

4.4 Bending Strength Characteristics

Bending strength (also known as flexural strength or modulus of rupture) is an indirect measure of the unreinforced mortar's tensile resistance and its ability to withstand bending moments before experiencing brittle fracture. Because mortar is relatively weak in tension compared to compression, the initiation of micro-cracks at the bottom fiber of the test prism dictates the ultimate failure. Figure 4.5 illustrates the bending strength of the plain mortar mixes at 28 days as a function of the Laterite replacement ratio.

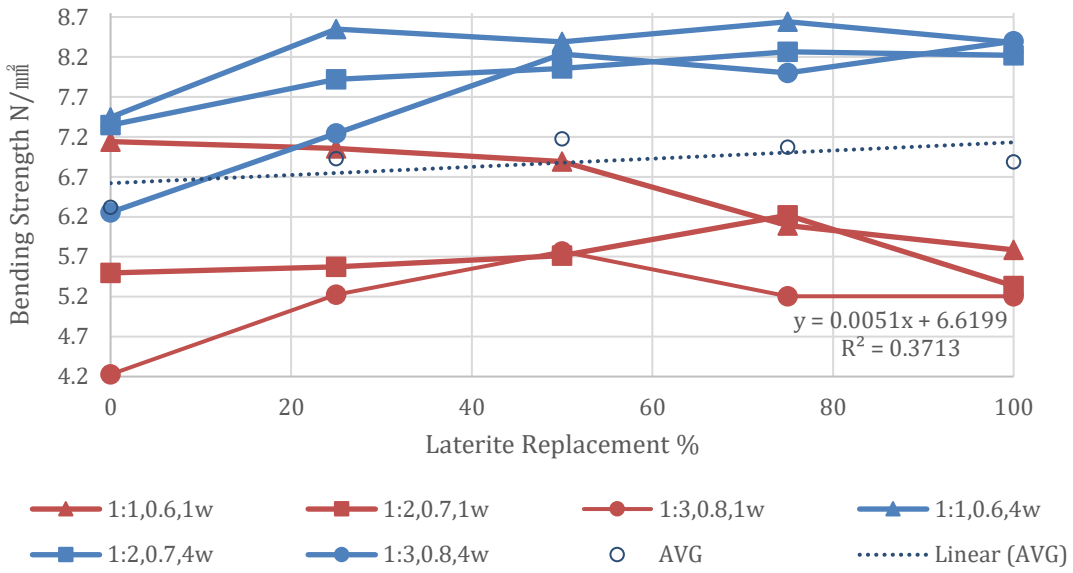

Fig 4.5: Bending Strength vs. Laterite Replacement Ratio

4.4.1 Plain Mix Flexural Behavior

The flexural behavior of the plain mixes closely mirrored the compressive strength trends, with one notable amplification. In the rich mix series (W/C 0.6), the bending strength not only remained stable but actually exhibited a slight, consistent increase as the laterite replacement ratio progressed toward 100%. This specific property enhancement is directly tied to the morphological characteristics of the crushed laterite aggregate.

River sand particles are naturally rounded and possess a smooth surface texture, which provides limited resistance against aggregate pull-out when subjected to tensile stresses in bending. Conversely, crushed laterite particles are highly irregular, jagged, and rough. When the abundant cement paste in the W/C 0.6 mix coats these particles, it creates a profound 'Mechanical Interlocking' effect. The aggregate serves to physically bridge micro-cracks and resist the pull-out forces. As a result, greater flexural energy is required to propagate a crack through the interlocking matrix, thereby elevating the bending strength.

However, this mechanical advantage relies entirely on the presence of a strong cementitious binder. In the lean mix series (W/C 0.8), the bending strength declined sharply at high replacement ratios. As dictated by the Paste Volume Theory, the inadequate volume of

cement paste was unable to fully coat the high surface area of the laterite fines. Without a continuous and robust binder phase to transfer the tensile stresses across the aggregate boundaries, the mechanical interlocking failed to engage, resulting in premature fracture.

4.4.2 Effect of Mineral Admixtures on Bending Strength

The application of mineral admixtures yielded intriguing results specifically concerning flexural behavior. Figure 4.6 compares the bending strength of the 100% Laterite mixes containing 15% Fly Ash (FA) and 15% Blast Furnace Slag (BF) against the plain control mix.

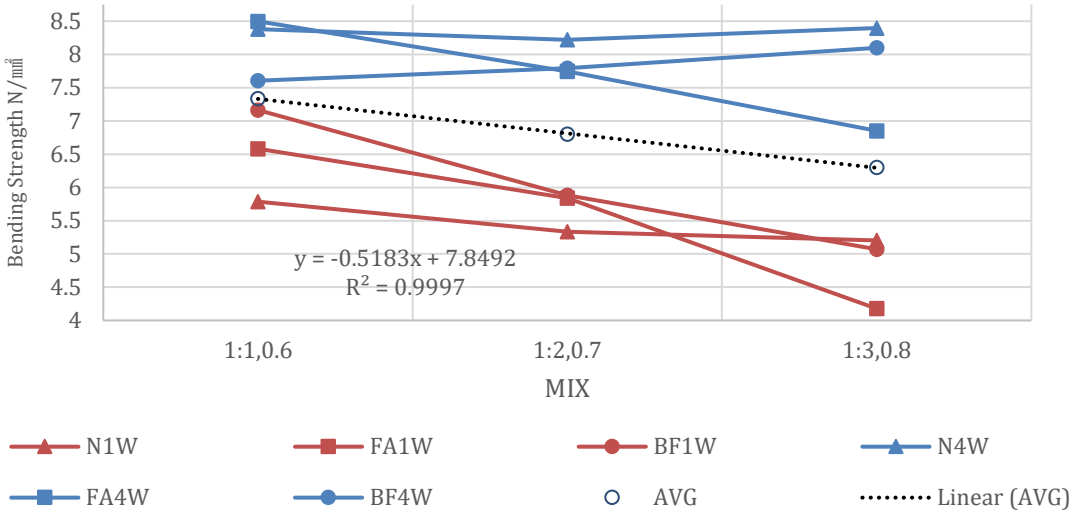

Fig 4.6: Effect of Admixtures on Bending Strength (100% Laterite)

An unexpected but scientifically significant anomaly was observed in the rich mix configuration (W/C 0.6). While Blast Furnace Slag dominated the compressive strength results (as previously discussed), the Fly Ash (FA) admixture slightly outperformed both the Plain mix and the BF mix in terms of bending strength. This divergence highlights the differing microstructural roles of the two admixtures.

The superior flexural performance of the Fly Ash mix can be attributed to its unique particle morphology. Fly ash consists of perfectly spherical, glassy particles. In the fresh state, these spheres improve the packing density and rheology of the mortar, allowing for excellent compaction around the highly irregular laterite particles. This reduces the size and frequency of macroscopic air voids where bending cracks typically initiate.

Furthermore, while the pozzolanic reaction of Fly Ash is too slow to drastically boost 28-day compressive crushing strength, the fine spherical particles act as a highly effective micro-filler. By physically occupying the microscopic gaps within the Interfacial Transition Zone (ITZ) without immediately creating a brittle, rigidly crystallized layer, the FA may introduce a slight degree of strain accommodation. This micro-level flexibility helps to distribute tensile stresses more evenly across the matrix under flexural loading, delaying crack propagation and marginally increasing the bending strength.

4.5 Splitting Tensile Strength

While compressive strength measures the material's resistance to crushing, splitting tensile strength evaluates the cohesive bond within the mortar matrix. Because concrete and mortar are inherently brittle materials, tensile failure is typically governed by the weakest link in the composite structure, which is almost exclusively the Interfacial Transition Zone (ITZ) between the aggregate surface and the cement paste. Figure 4.7 presents the 28-day splitting tensile strength of the plain mortar mixes.

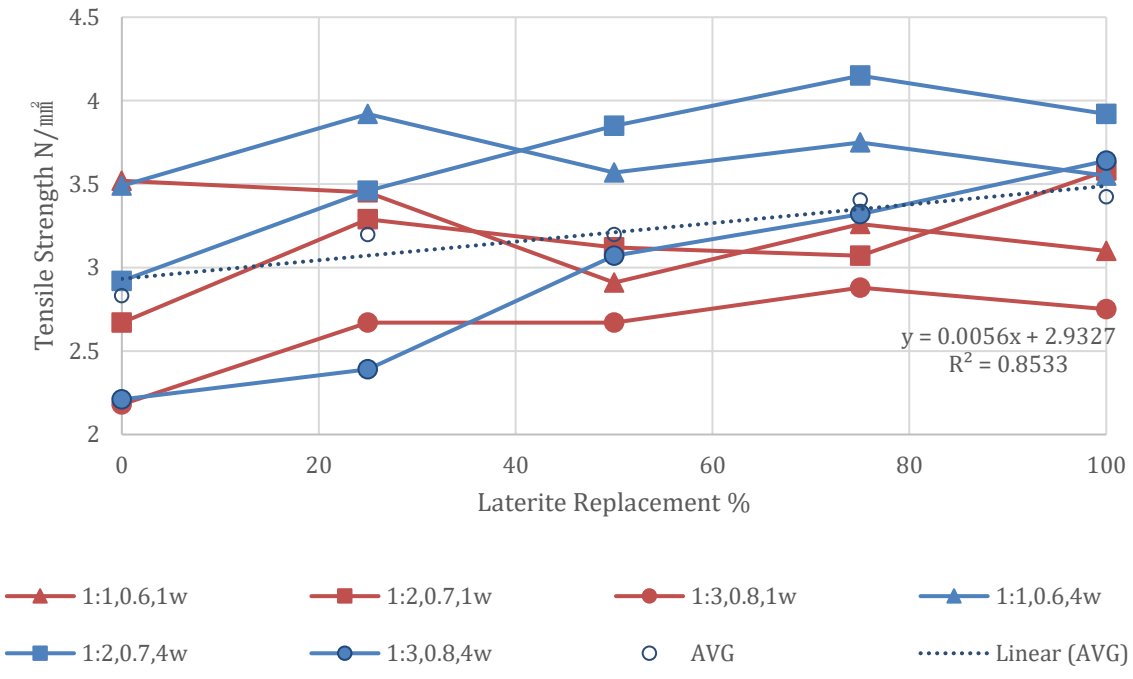

Fig 4.7: Splitting Tensile Strength vs. Laterite Replacement Ratio

4.5.1 Plain Mix Tensile Behavior and Mechanical Interlocking

A highly significant observation from the tensile testing data is the comparative resilience of the laterite mixtures. While the compressive strength of the lean mix (W/C 0.8) suffered a severe drop at high replacement ratios, the splitting tensile strength did not degrade with the same severity. Across the tested specimens, the tensile strength maintained a remarkably consistent ratio of approximately 1/10th of the compressive strength, ranging from 2.0 to 4.0 N/mm^2.

This resilience directly validates the 'Mechanical Interlocking' hypothesis. River sand, shaped by centuries of aquatic erosion, possesses a smooth, rounded morphology. Under tensile stress, the smooth interface provides minimal friction, allowing the cement paste to debond and pull away cleanly. Crushed laterite, however, is characterized by jagged edges, angular morphologies, and a highly irregular, vesicular surface texture.

When the cementitious binder hydrates, it physically infiltrates these microscopic surface crevices. Upon hardening, the paste is geometrically 'keyed' into the aggregate. When a diametrical splitting force is applied to the cylinder, this interlocking interface strongly resists separation. The mechanical friction provided by the laterite surface essentially arrests micro-crack propagation at the ITZ. Consequently, the mortar matrix exhibits a higher capacity to bridge tensile stresses before ultimate macroscopic failure occurs. This indicates that while the porosity of laterite limits the maximum crushing load, its surface roughness is exceptionally beneficial for maintaining structural cohesion under tension.

4.5.2 Effect of Mineral Admixtures on Tensile Strength

To further fortify the aggregate-paste bond, 15% of the cement was replaced with Fly Ash (FA) and Blast Furnace Slag (BF) in the 100% laterite mixtures. The splitting tensile strength results for these admixture series at 28 days are illustrated in Figure 4.8.

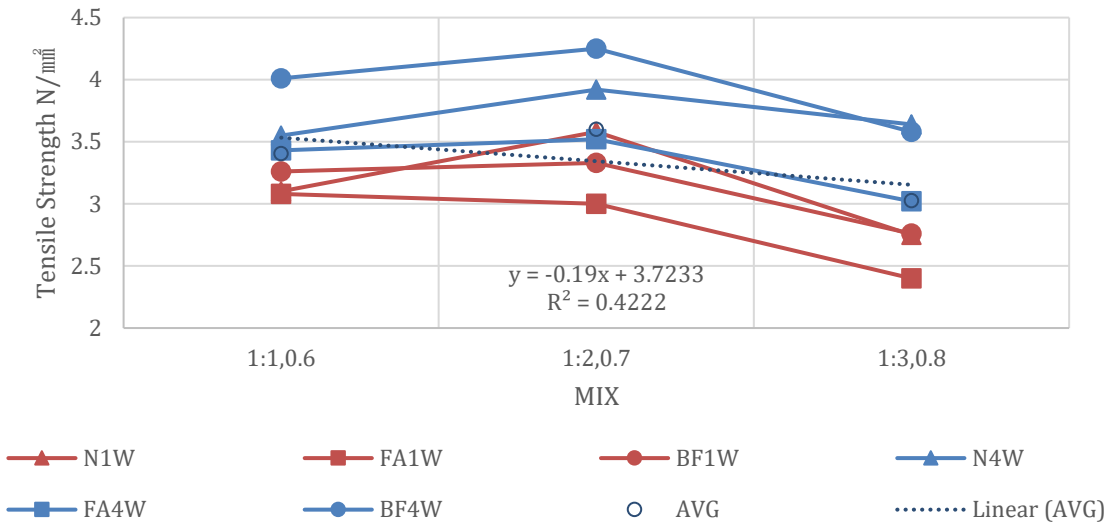

Fig 4.8: Effect of Admixtures on Splitting Tensile Strength (100% Laterite)

The data clearly demonstrates that the addition of Blast Furnace Slag (BF) yielded superior tensile reinforcement. Across all W/C ratios, the BF Slag mixes outperformed both the Plain and Fly Ash variants. For instance, at W/C 0.6, the tensile strength increased significantly with the application of slag, reaching up to 4.28 N/mm².

The mechanism driving this improvement is the densification of the ITZ through latent hydraulic activity. The highly alkaline environment of the Portland cement activates the fine slag particles. As the slag hydrates, it produces an abundance of secondary Calcium Silicate Hydrate (C-S-H) gel. Because the laterite particles possess open surface pores, this secondary C-S-H gel precipitates directly inside the aggregate's outer voids. This process chemically and physically 'welds' the laterite to the surrounding paste, eliminating the weak boundary layer that typically initiates tensile failure [5].

In contrast, the Fly Ash (FA) mixes exhibited tensile strengths that were comparable to, or slightly lower than, the plain control mixes at 28 days (e.g., 3.43 N/mm² at W/C 0.6). As discussed in the theoretical background, the pozzolanic reaction of Fly Ash is a slow process dependent on the gradual accumulation of Calcium Hydroxide. Within the 28-day curing window of this study, the Fly Ash particles primarily acted as inert micro-fillers, improving fresh state packing but not yet contributing the chemical bonds necessary to elevate tensile resistance.

4.6 Tested specimen and all of the calculated data

4.6.1 Data and pictures of tested specimens at the 1-week mark

Mold Specimen (FA 1 Week)

Test Failure
Chip/Dent

Specimen		W/C	C:A	S:L	Dimensions (mm)		Max Load (kN)				Strength (N/mm²)			
					Width b	Height h	Bending	Compression			Bending Strength	Bending Strength (Avg)	Comp. Strength	Comp. Strength (Avg)
								①	②	Average				
No. 1	1-①	0.6	1:1	0:100	40.10	40.05	3.40	48.46	52.98	50.72	7.888	7.416	31.581	31.432
	1-②				40.10	40.05	3.12	53.77	52.82	53.30	7.238		33.188	
	1-③				40.10	40.05	3.07	45.50	49.35	47.42	7.122		29.527	
No. 6	6-①	0.7	1:2	0:100	40.10	40.05	3.39	53.94		49.73	7.865	7.416	30.965	31.058
	6-②				40.10	40.05	2.99	54.24	45.47	49.86	6.937		31.046	
	6-③				40.10	40.05	3.21	50.33	49.77	50.05	7.447		31.164	
No. 11	11-①	0.7	1:2	0:100	40.10	40.05	2.58	47.35	45.58	46.47	5.986	5.608	28.935	27.226
	11-②				40.10	40.05	2.82	52.97	52.66	52.81	6.542		32.883	
	11-③				40.05	40.05	1.84	30.85	32.70	31.78	4.296		19.859	

Mold Specimen (BF 1 Week)

Test Failure
Chip/Dent

Specimen		W/C	C:A	S:L	Dimensions (mm)		Max Load (kN)				Strength (N/mm²)			
					Width b	Height h	Bending	Compression			Bending Strength	Bending Strength (Avg)	Comp. Strength	Comp. Strength (Avg)
								①	②	Average				
No. 1	1-①	0.6	1:1	0:100	40.10	40.05	2.66	53.84	45.17	49.51	6.171	6.287	30.828	29.821
	1-②				40.10	40.05	2.72	45.57	45.90	45.73	6.310		28.474	
	1-③				40.10	40.05	2.75	50.57	46.30	48.44	6.380		30.162	
No. 6	6-①	0.7	1:2	0:100	40.10	40.05	3.08	49.55	50.20	49.88	7.146	6.836	31.058	32.615
	6-②				40.10	40.05	3.14	54.46	54.41	54.44	7.285		33.898	
	6-③				40.10	40.05	2.62	53.94	51.70	52.82	6.078		32.889	
No. 11	11-①	0.7	1:2	0:100	40.10	40.05	2.97	53.57	50.62	52.09	6.890	6.821	32.435	32.354
	11-②				40.10	40.05	2.65	54.76	51.56	53.16	6.148		33.101	
	11-③				40.10	40.05	3.20	51.51	49.76	50.63	7.424		31.525	

FA 1 Week

Test Failure	Specimen		W/C	C:A	S:L	Mass Before Drying (g)	Mass After Drying (g)	Mass Loss (g)	Water Absorption (%)	Avg Water Absorption (%)	Diameter ① (mm)	Diameter ② (mm)	Avg Diameter (mm)	Height (mm)	Volume (cm³)	Density (g/cm³)	Avg Density (g/cm³)	Max Load (kN)	Tensile Strength (N/mm²)	Avg Tensile Strength (N/mm²)
Chip/Dent	No. 1	④	0.6	1:1	0:100	381.3	342.8	38.5	11.231	11.426	50.16	50.03	50.095	98.90	194.9	1.96	2.04	23.53	3.02	3.08
		⑤				408.4	361.3	47.1	13.036		50.04	50.01	50.025	98.06	192.7	2.12		21.99	2.85	
		⑥				397.8	361.6	36.2	10.011		50.11	50.24	50.175	98.26	194.3	2.05		26.11	3.37	
	No. 6	④	0.7	1:2	0:100	375.5	338.9	36.6	10.800	11.113	50.23	50.23	50.230	94.19	186.6	2.01	2.01	34.10	4.59	4.48
		⑤				383.9	344.6	39.3	11.405		50.21	50.22	50.215	98.85	195.8	1.96		34.38	4.41	
		⑥				383.3	344.9	38.4	11.134		50.12	50.12	50.120	94.79	187.0	2.05		33.04	4.43	
	No. 11	④	0.7	1:2	0:100	388.0	328.6	59.4	18.077	13.799	50.05	50.00	50.025	96.65	190.0	2.04	2.06	19.62	2.58	3.33
		⑤				395.0	350.5	44.5	12.696		50.15	50.18	50.165	94.57	186.9	2.11		24.19	3.25	
		⑥				391.5	353.9	37.6	10.624		50.08	50.07	50.075	97.42	191.9	2.04		31.84	4.16	

BF1 Week

Test Failure	Specimen		W/C	C:A	S:L	Mass Before Drying (g)	Mass After Drying (g)	Mass Loss (g)	Water Absorption (%)	Avg Water Absorption (%)	Diameter ① (mm)	Diameter ② (mm)	Avg Diameter (mm)	Height (mm)	Volume (cm³)	Density (g/cm³)	Avg Density (g/cm³)	Max Load (kN)	Tensile Strength (N/mm²)	Avg Tensile Strength (N/mm²)
Chip/Dent	No. 1	④	0.6	1:1	0:100	395.8	344.3	51.5	14.958	14.379	50.15	50.09	50.120	94.83	187.1	2.12	2.07	21.40	2.87	3.46
		⑤				377.0	331.4	45.6	13.760		50.10	50.15	50.125	95.72	188.9	2.00		23.49	3.12	
		⑥				402.3	351.6	50.7	14.420		50.00	50.18	50.090	97.27	191.7	2.10		33.56	4.39	
	No. 6	④	0.7	1:2	0:100	388.8	336.4	52.4	15.577	12.553	50.17	50.12	50.145	98.74	195.0	1.99	2.07	34.23	4.40	3.95
		⑤				402.4	366.9	35.5	9.676		50.12	50.05	50.085	94.05	185.3	2.17		27.14	3.67	
		⑥				391.4	348.2	43.2	12.407		50.20	50.17	50.185	97.08	192.0	2.04		28.82	3.77	
	No. 11	④	0.7	1:2	0:100	412.4	356.6	55.8	15.648	14.087	50.03	50.00	50.015	96.16	188.9	2.18	2.12	23.20	3.07	3.38
		⑤				405.8	365.3	40.5	11.087		50.16	50.04	50.100	95.18	187.6	2.16		27.32	3.65	
		⑥				388.4	336.2	52.2	15.526		50.24	50.25	50.245	97.26	192.8	2.01		26.23	3.42	

Blast Furnace Slag mix **Fly Ash mix**

Test Failure
Chip/Dent

Mold Specimen (1 Week)

Specimen		W/C	C:A	S:L	Dimensions (mm)		Max Load (kN)				Strength (N/mm²)			
					Width b	Height h	Bending	Compression			Bending Strength	Bending Strength (Avg)	Comp. Strength	Comp. Strength (Avg)
								①	②	Average				
No. 1	1-①	0.6	1:1	0:100	40.10	40.05	2.94	52.12	46.30	49.21	6.821	7.262	30.641	30.927
	1-②				40.10	40.05	3.32	46.94	50.34	48.64	7.702		30.286	
	1-③				40.10	40.05	3.13	50.31	52.00	51.16	7.262		31.855	
No. 2	2-①	0.6	1:1	25:75	40.10	40.05	3.07	46.80	46.49	46.64	7.122	6.364	29.041	31.477
	2-②				40.10	40.05	2.63	52.75	53.28	53.02	6.102		33.014	
	2-③				40.10	40.00	2.51	28.88	51.80	51.80	5.868		32.375	
No. 3	3-①	0.6	1:1	50:50	40.10	40.05	2.89	51.93	47.75	49.84	6.705	6.852	31.034	29.531
	3-②				40.10	40.05	2.90	45.35	47.70	46.53	6.728		28.973	
	3-③				40.10	40.05	3.07	46.15	45.67	45.91	7.122		28.586	
No. 4	4-①	0.6	1:1	75:25	40.10	40.05	3.24	47.44	45.59	46.52	7.517	6.821	28.966	30.616
	4-②				40.10	40.05	3.05	54.21	54.70	54.45	7.076		33.904	
	4-③				40.10	40.05	2.53	47.70	45.38	46.54	5.870		28.979	
No. 5	5-①	0.6	1:1	100:0	39.90	40.20	3.26	46.70	44.95	45.83	7.584	7.339	28.712	30.820
	5-②				39.95	40.15	2.88	53.10	49.45	51.28	6.708		32.087	
	5-③				40.10	40.05	3.33	52.90	48.80	50.85	7.726		31.662	
No. 6	6-①	0.7	1:2	0:100	40.10	40.05	3.18	54.13	49.52	51.83	7.378	7.780	32.273	31.144
	6-②				40.10	40.05	3.40	47.38	46.84	47.11	7.888		29.334	
	6-③				40.10	40.05	3.48	51.98	50.25	51.11	8.074		31.824	
No. 7	7-①	0.7	1:2	25:75	40.10	40.05	2.68	47.74	48.83	48.28	6.218	7.192	30.062	31.436
	7-②				40.10	40.05	3.42	52.73	51.19	51.96	7.934		32.354	
	7-③				40.10	40.05	3.20	52.12	50.32	51.22	7.424		31.893	
No. 8	8-①	0.7	1:2	50:50	40.10	40.05	2.92	49.77	49.97	49.87	6.774	6.751	31.052	31.094
	8-②				40.10	40.05	2.98	47.82	48.23	48.02	6.914		29.900	
	8-③				40.10	40.05	2.83	49.90	53.95	51.92	6.566		32.329	
No. 9	9-①	0.7	1:2	75:25	40.10	40.05	3.17	53.36	51.05	52.20	7.354	7.277	32.503	30.847
	9-②				40.10	40.05	2.75	48.07	45.79	46.93	6.380		29.222	
	9-③				40.10	40.05	3.49	50.50	48.48	49.49	8.097		30.816	
No. 10	10-①	0.7	1:2	100:0	40.10	40.05	3.10	50.24	45.73	47.98	7.192	6.464	29.875	29.645
	10-②				40.10	40.05	2.85	52.48	48.14	50.31	6.612		31.326	
	10-③				40.10	40.00	2.39	45.10	43.65	44.38	5.588		27.734	
No. 11	11-①	0.7	1:2	0:100	40.10	40.05	2.96	51.57	54.30	52.94	6.867	6.960	32.964	31.542
	11-②				40.10	40.05	3.40	46.86	52.11	49.48	7.888		30.809	
	11-③				40.10	40.05	2.64	48.60	50.51	49.55	6.125		30.853	
No. 12	12-①	0.8	1:3	25:75	40.10	40.00	2.23	43.05	42.45	42.75	5.214	6.981	26.719	30.073
	12-②				40.10	40.05	3.49	54.43	45.90	50.16	8.097		31.233	
	12-③				40.10	40.05	3.29	51.57	52.07	51.82	7.633		32.266	
No. 13	13-①	0.8	1:3	50:50	40.10	40.05	3.08	46.98	52.32	49.65	7.146	6.981	30.915	29.246
	13-②				40.15	40.00	2.55	44.35	45.55	44.95	5.954		28.094	
	13-③				40.10	40.05	3.38	45.01	47.27	46.14	7.842		28.730	
No. 14	14-①	0.8	1:3	75:25	40.10	40.05	3.37	50.94	52.06	51.50	7.818	7.517	32.067	32.117
	14-②				40.10	40.05	2.93	48.29	54.51	51.40	6.798		32.005	
	14-③				40.10	40.05	3.42	51.20	52.48	51.84	7.934		32.279	
No. 15	15-①	0.8	1:3	100:0	40.10	40.05	2.85	49.15	47.39	48.27	6.612	6.550	30.056	29.647
	15-②				40.10	40.05	2.91	48.08	49.89	48.98	6.751		30.498	
	15-③				40.10	40.05	2.71	45.29	45.88	45.59	6.287		28.387	

1 Week

Test Failure	Specimen		W/C	C:A	S:L	Mass Before Drying (g)	Mass After Drying (g)	Mass Loss (g)	Water Absorption (%)	Avg Water Absorption (%)	Diameter ① (mm)	Diameter ② (mm)	Avg Diameter (mm)	Height (mm)	Volume (cm^3)	Density (g/cm^3)	Avg Density (g/cm^3)	Max Load (kN)	Tensile Strength (N/mm^2)	Avg Tensile Strength (N/mm^2)
Chip/Dent		④				383.7	335.5	48.2	14.367		50.21	50.19	50.200	98.83	195.6	1.96		23.50	3.02	
	No. 1	⑤	0.6	1:1	0:100	397.4	346.4	51.0	14.723	14.773	50.23	50.22	50.225	94.19	186.6	2.13	2.06	28.38	3.82	3.73
		⑥				401.8	348.7	53.1	15.228		50.01	50.02	50.015	97.82	192.2	2.09		33.44	4.35	
		④				400.3	341.2	59.1	17.321		50.05	50.07	50.060	98.26	193.4	2.07		20.22	2.62	
	No. 2	⑤	0.6	1:1	25:75	394.7	336.1	58.6	17.435	16.170	50.06	50.11	50.085	94.99	187.1	2.11	2.08	30.43	4.07	3.60
		⑥				397.8	349.7	48.1	13.755		50.20	50.07	50.135	97.75	193.0	2.06		31.73	4.12	
		④				395.2	354.1	41.1	11.607		50.23	50.01	50.120	95.55	188.5	2.10		21.93	2.92	
	No. 3	⑤	0.6	1:1	50:50	407.3	355.6	51.7	14.539	14.933	50.11	50.10	50.105	97.13	191.5	2.13	2.08	32.60	4.26	3.47
		⑥				377.2	317.9	59.3	18.654		50.07	50.11	50.090	95.59	188.4	2.00		24.28	3.23	
		④				377.3	323.8	53.5	16.523		50.14	50.01	50.075	97.28	191.6	1.97		29.37	3.84	
	No. 4	⑤	0.6	1:1	75:25	403.6	368.2	35.4	9.614	14.406	50.18	50.18	50.180	96.19	190.2	2.12	2.09	33.88	4.47	4.20
		⑥				405.8	346.6	59.2	17.080		50.05	50.02	50.035	94.22	185.3	2.19		31.75	4.29	
		④				404.1	351.6	52.5	14.932		50.01	50.11	50.060	94.97	186.9	2.16		32.48	4.35	
	No. 5	⑤	0.6	1:1	100:0	375.4	333.1	42.3	12.699	14.110	50.03	50.12	50.075	96.51	190.1	1.97	2.07	27.57	3.63	3.81
		⑥				399.5	348.3	51.2	14.700		50.13	50.04	50.085	97.88	192.8	2.07		26.53	3.45	
		④				403.6	353.8	49.8	14.076		50.04	50.03	50.035	95.44	187.7	2.15		29.85	3.98	
	No. 6	⑤	0.7	1:2	0:100	385.1	347.1	38.0	10.948	11.846	50.18	50.13	50.155	98.05	193.7	1.99	2.08	29.68	3.84	3.66
		⑥				394.2	356.7	37.5	10.513		50.11	50.02	50.065	94.91	186.8	2.11		23.66	3.17	
		④				394.3	352.9	41.4	11.731		50.18	50.22	50.200	94.98	188.0	2.10		33.18	4.43	
	No. 7	⑤	0.7	1:2	25:75	399.7	342.1	57.6	16.837	14.448	50.21	50.11	50.160	97.43	192.5	2.08	2.10	20.37	2.65	3.69
		⑥				408.6	356.0	52.6	14.775		50.04	50.15	50.095	97.34	191.9	2.13		30.52	3.98	
		④				379.4	326.7	52.7	16.131		50.11	50.16	50.135	98.38	194.2	1.95		26.32	3.40	
	No. 8	⑤	0.7	1:2	50:50	394.4	338.0	56.4	16.686	15.233	50.05	50.24	50.145	95.04	187.7	2.10	2.01	27.65	3.69	3.52
		⑥				380.3	336.9	43.4	12.882		50.13	50.03	50.080	97.76	192.6	1.97		26.71	3.47	
		④				391.9	345.7	46.2	13.364		50.00	50.05	50.025	98.29	193.2	2.03		33.74	4.37	
	No. 9	⑤	0.7	1:2	75:25	410.0	356.2	53.8	15.104	12.754	50.22	50.00	50.110	98.32	193.9	2.11	2.07	25.70	3.32	3.93
		⑥				393.5	358.4	35.1	9.794		50.17	50.06	50.115	96.04	189.4	2.08		31.06	4.11	
		④				398.3	340.2	58.1	17.078		50.22	50.20	50.210	98.69	195.4	2.04		27.78	3.57	
	No. 10	⑤	0.7	1:2	100:0	404.7	358.3	46.4	12.950	16.079	50.08	50.13	50.105	94.13	185.6	2.18	2.09	26.51	3.58	3.54
		⑥				388.2	328.4	59.8	18.210		50.17	50.23	50.200	95.45	188.9	2.06		26.20	3.48	
		④				411.5	375.1	36.4	9.704		50.14	50.00	50.070	94.98	187.0	2.20		23.13	3.10	
	No. 11	⑤	0.7	1:2	0:100	375.0	335.7	39.3	11.707	12.202	50.06	50.10	50.080	96.67	190.4	1.97	2.10	25.17	3.31	3.07
		⑥				405.6	352.1	53.5	15.195		50.20	50.10	50.150	96.70	191.0	2.12		21.28	2.79	
		④				396.4	358.9	37.5	10.449		50.24	50.03	50.135	96.67	190.8	2.08		24.49	3.22	
	No. 12	⑤	0.8	1:3	25:75	392.1	333.5	58.6	17.571	12.904	50.22	50.15	50.185	98.22	194.3	2.02	2.09	27.27	3.52	3.16
		⑥				404.8	365.7	39.1	10.692		50.20	50.02	50.110	94.11	185.6	2.18		20.39	2.75	
		④				408.7	359.5	49.2	13.686		50.25	50.01	50.130	96.51	190.5	2.15		21.35	2.81	
	No. 13	⑤	0.8	1:3	50:50	405.9	369.0	36.9	10.000	12.367	50.17	50.05	50.110	95.17	187.7	2.16	2.11	28.27	3.77	3.54
		⑥				381.3	336.2	45.1	13.415		50.11	50.14	50.125	96.30	190.0	2.01		30.52	4.03	
		④				406.6	353.9	52.7	14.891		50.09	50.25	50.170	96.96	191.7	2.12		33.86	4.43	
	No. 14	⑤	0.8	1:3	75:25	412.4	360.8	51.6	14.302	14.882	50.11	50.08	50.095	97.08	191.3	2.16	2.10	32.17	4.21	3.94
		⑥				397.5	344.3	53.2	15.452		50.13	50.22	50.175	98.99	195.7	2.03		24.84	3.18	
		④				378.9	321.7	57.2	17.781		50.06	50.22	50.140	95.28	188.1	2.01		30.09	4.01	
	No. 15	⑤	0.8	1:3	100:0	414.8	366.3	48.5	13.241	13.698	50.24	50.12	50.180	96.83	191.5	2.17	2.09	25.90	3.39	3.96
		⑥				404.4	367.4	37.0	10.071		50.23	50.04	50.135	98.53	194.5	2.08		34.65	4.47	

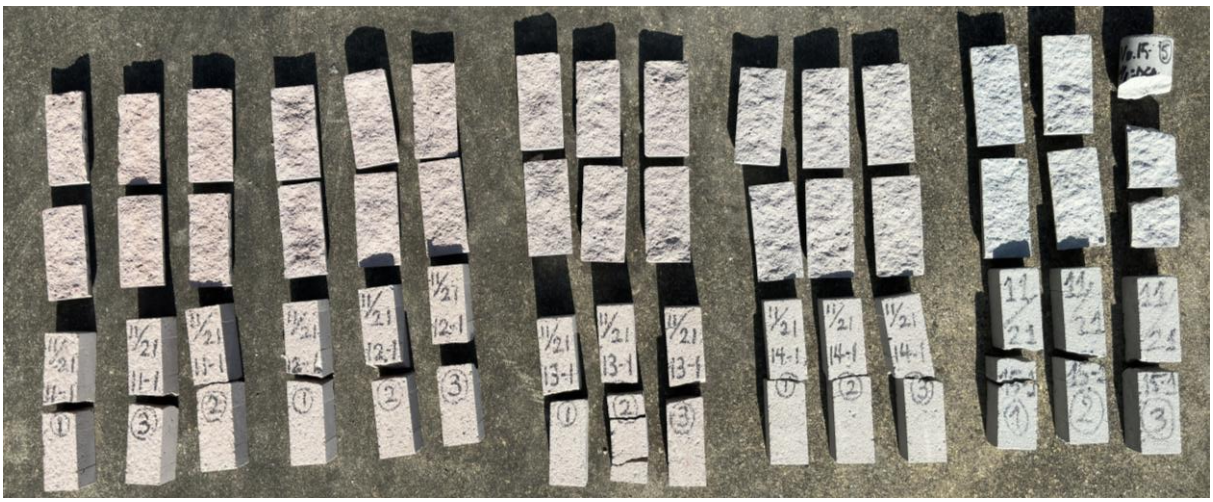

A/C:3/1-W/C:0.8

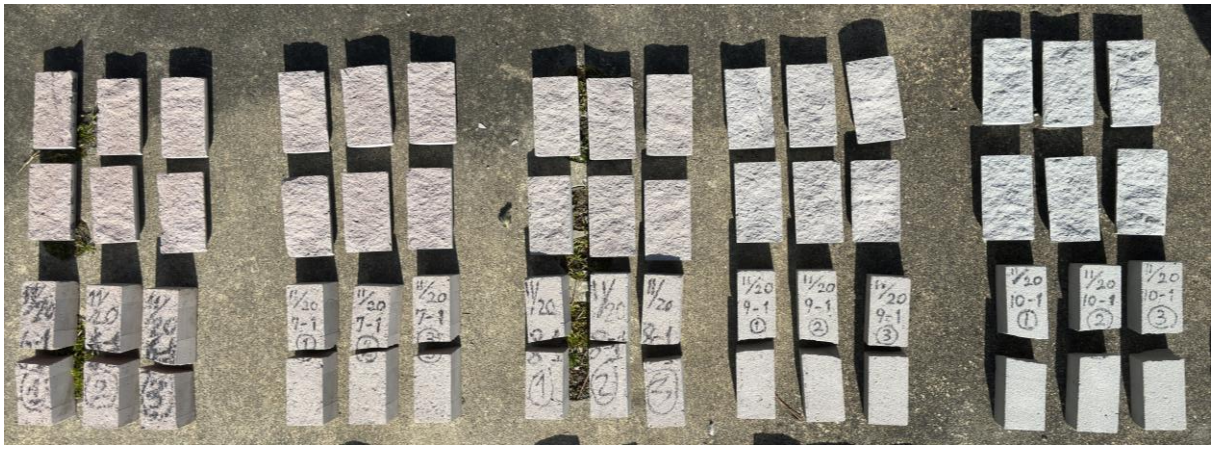

A/C:2/1-W/C:0.7

A/C:1/1-W/C:0.6

4.6.2 Data and pictures of tested specimens at the 4-week mark

Mold Specimen (FA 4 Weeks)

Test Failure
Chip/Dent

Specimen		W/C	C:A	S:L	Dimensions (mm)		Max Load (kN)				Strength (N/mm²)			
					Width b	Height h	Bending	Compression			Bending Strength	Bending Strength (Avg)	Comp. Strength	Comp. Strength (Avg)
								①	②	Average				
No. 1	1-①	0.6	1:1	0:100	40.10	40.05	3.44	54.59	46.22	50.41	7.981	7.215	31.388	30.871
	1-②				40.10	40.05	2.86	48.78	48.93	48.86	6.635		30.423	
	1-③				40.10	40.05	3.03	46.67	52.27	49.47	7.030		30.803	
No. 6	6-①	0.7	1:2	0:100	40.10	40.05	2.94	47.17	49.67	48.42	6.821	6.682	30.149	31.148
	6-②				40.10	40.05	2.57	48.22	53.33	50.77	5.962		31.613	
	6-③				40.10	40.05	3.13	53.13	48.62	50.88	7.262		31.681	
No. 11	11-①	0.7	1:2	0:100	40.20	40.10	2.87	47.25	49.00	48.13	6.651	7.275	30.079	30.971
	11-②				40.10	40.05	3.19	53.22	49.88	51.55	7.401		32.098	
	11-③				40.10	40.05	3.35	50.22	48.49	49.36	7.772		30.735	

Mold Specimen (BF 4 Weeks)

Test Failure
Chip/Dent

Specimen		W/C	C:A	S:L	Dimensions (mm)		Max Load (kN)				Strength (N/mm²)			
					Width b	Height h	Bending	Compression			Bending Strength	Bending Strength (Avg)	Comp. Strength	Comp. Strength (Avg)
								①	②	Average				
No. 1	1-①	0.6	1:1	0:100	40.10	40.05	2.54	50.33	54.07	52.20	5.893	6.543	32.503	32.231
	1-②				40.10	40.05	3.39	48.94	51.71	50.33	7.865		31.339	
	1-③				40.10	40.05	2.53	54.52	50.99	52.76	5.870		32.852	
No. 6	6-①	0.7	1:2	0:100	40.10	40.05	2.94	46.50	49.06	47.78	6.821	7.370	29.751	31.328
	6-②				40.10	40.05	3.13	52.26	51.16	51.71	7.262		32.198	
	6-③				40.10	40.05	3.46	48.35	54.54	51.45	8.027		32.036	
No. 11	11-①	0.7	1:2	0:100	40.20	40.10	3.32	59.15	61.45	60.30	7.704	7.927	37.688	33.094
	11-②				40.10	40.05	3.50	45.21	52.81	49.01	8.120		30.517	
	11-③				40.10	40.05	3.43	48.26	51.57	49.91	7.958		31.077	

FA 4 Weeks

Test Failure
Chip/Dent

Specimen		W/C	C:A	S:L	Mass Before Drying (g)	Mass After Drying (g)	Mass Loss (g)	Water Absorption (%)	Avg Water Absorption (%)	Diameter ① (mm)	Diameter ② (mm)	Avg Diameter (mm)	Height (mm)	Volume (cm³)	Density (g/cm³)	Avg Density (g/cm³)	Max Load (kN)	Tensile Strength (N/mm²)	Avg Tensile Strength (N/mm²)
No. 1	④	0.6	1:1	0:100	406.8	353.9	52.9	14.948	14.378	50.10	50.06	50.080	95.45	188.0	2.16	2.12	24.99	3.33	3.19
	⑤				405.9	350.4	55.5	15.839		50.15	50.18	50.165	96.83	191.4	2.12		20.53	2.69	
	⑥				404.0	359.6	44.4	12.347		50.01	50.03	50.020	98.36	193.3	2.09		27.47	3.55	
No. 6	④	0.7	1:2	0:100	386.8	331.9	54.9	16.541	14.974	50.13	50.04	50.085	98.91	194.9	1.98	2.02	31.61	4.06	3.45
	⑤				380.3	323.3	57.0	17.631		50.12	50.16	50.140	96.82	191.2	1.99		21.15	2.77	
	⑥				400.8	361.9	38.9	10.749		50.14	50.13	50.135	96.76	191.0	2.10		26.72	3.51	
No. 11	④	0.7	1:2	0:100	410.6	358.1	52.5	14.661	15.513	50.20	50.24	50.220	98.56	195.2	2.10	2.10	33.57	4.32	4.47
	⑤				398.7	351.5	47.2	13.428		50.21	50.09	50.150	94.76	187.2	2.13		32.84	4.40	
	⑥				383.3	323.6	59.7	18.449		50.24	50.20	50.220	94.11	186.4	2.06		34.91	4.70	

BF 4 Weeks

Test Failure
Chip/Dent

Specimen		W/C	C:A	S:L	Mass Before Drying (g)	Mass After Drying (g)	Mass Loss (g)	Water Absorption (%)	Avg Water Absorption (%)	Diameter ① (mm)	Diameter ② (mm)	Avg Diameter (mm)	Height (mm)	Volume (cm³)	Density (g/cm³)	Avg Density (g/cm³)	Max Load (kN)	Tensile Strength (N/mm²)	Avg Tensile Strength (N/mm²)
No. 1	④	0.6	1:1	0:100	382.3	345.6	36.7	10.619	11.440	50.19	50.16	50.175	98.82	195.4	1.96	2.02	25.45	3.27	3.31
	⑤				382.3	340.7	41.6	12.210		50.02	50.00	50.010	98.79	194.1	1.97		22.48	2.90	
	⑥				405.6	363.8	41.8	11.490		50.00	50.01	50.005	96.38	189.3	2.14		28.44	3.76	
No. 6	④	0.7	1:2	0:100	399.3	348.2	51.1	14.675	16.338	50.21	50.02	50.115	95.90	189.2	2.11	2.08	30.63	4.06	3.95
	⑤				409.1	350.9	58.2	16.586		50.15	50.10	50.125	98.72	194.8	2.10		34.04	4.38	
	⑥				379.4	322.2	57.2	17.753		50.00	50.03	50.015	94.88	186.4	2.04		25.35	3.40	
No. 11	④	0.7	1:2	0:100	411.9	355.6	56.3	15.832	14.989	50.06	50.01	50.035	98.26	193.2	2.13	2.06	31.61	4.09	3.95
	⑤				376.4	336.2	40.2	11.957		50.16	50.06	50.110	94.55	186.5	2.02		34.49	4.63	
	⑥				386.8	330.1	56.7	17.177		50.23	50.12	50.175	96.79	191.4	2.02		23.97	3.14	

Blast Furnace Slag mix

Fly Ash mix

Test Failure
Chip/Dent

Mold Specimen (4 Weeks)

Specimen		W/C	C:A	S:L	Dimensions (mm)		Max Load (kN)				Strength (N/mm²)			
					Width b	Height h	Bending	Compression			Bending Strength	Bending Strength (Avg)	Comp. Strength	Comp. Strength (Avg)
								①	②	Average				
No. 1	1-①	0.6	1:1	0:100	40.10	40.05	3.02	45.72	54.28	50.00	7.006	6.712	31.133	31.060
	1-②				40.10	40.05	2.65	45.13	52.21	48.67	6.148		30.305	
	1-③				40.10	40.05	3.01	47.62	54.34	50.98	6.983		31.743	
No. 2	2-①	0.6	1:1	25:75	40.10	40.05	2.82	45.42	49.66	47.54	6.542	6.921	29.601	29.917
	2-②				40.10	40.05	2.69	45.37	45.51	45.44	6.241		28.294	
	2-③				40.10	40.05	3.44	48.15	54.18	51.16	7.981		31.855	
No. 3	3-①	0.6	1:1	50:50	40.10	40.05	3.09	48.51	49.05	48.78	7.169	6.728	30.374	30.164
	3-②				40.10	40.05	2.53	53.18	48.25	50.72	5.870		31.581	
	3-③				40.10	40.05	3.08	45.71	45.95	45.83	7.146		28.537	
No. 4	4-①	0.6	1:1	75:25	40.10	40.05	3.45	50.03	54.65	52.34	8.004	7.741	32.590	30.915
	4-②				40.10	40.05	3.48	45.54	46.01	45.77	8.074		28.499	
	4-③				40.10	40.05	3.08	49.17	52.52	50.84	7.146		31.656	
No. 5	5-①	0.6	1:1	100:0	40.10	40.05	3.18	46.40	48.15	47.27	7.378	7.084	29.433	31.044
	5-②				40.10	40.05	2.74	53.88	51.62	52.75	6.357		32.845	
	5-③				40.10	40.05	3.24	47.56	51.55	49.55	7.517		30.853	
No. 6	6-①	0.7	1:2	0:100	40.10	40.05	2.96	47.16	53.97	50.56	6.867	6.890	31.482	30.571
	6-②				40.10	40.05	3.23	45.32	48.66	46.99	7.494		29.259	
	6-③				40.10	40.05	2.72	50.26	49.22	49.74	6.310		30.971	
No. 7	7-①	0.7	1:2	25:75	40.10	40.05	3.26	50.84	45.42	48.13	7.563	7.726	29.969	31.042
	7-②				40.10	40.05	3.25	54.37	48.33	51.35	7.540		31.974	
	7-③				40.10	40.05	3.48	53.51	46.64	50.08	8.074		31.183	
No. 8	8-①	0.7	1:2	50:50	40.10	40.05	3.08	48.23	54.94	51.58	7.146	7.494	32.117	32.831
	8-②				40.10	40.05	3.31	53.68	54.81	54.25	7.679		33.779	
	8-③				40.10	40.05	3.30	53.26	51.44	52.35	7.656		32.596	
No. 9	9-①	0.7	1:2	75:25	40.10	40.05	2.88	46.69	45.38	46.03	6.682	6.705	28.661	30.031
	9-②				40.10	40.05	3.19	49.37	51.78	50.58	7.401		31.494	
	9-③				40.10	40.05	2.60	50.71	45.45	48.08	6.032		29.938	
No. 10	10-①	0.7	1:2	100:0	40.10	40.05	3.40	45.09	52.84	48.97	7.888	7.246	30.492	30.994
	10-②				40.10	40.05	3.32	54.77	46.82	50.80	7.702		31.631	
	10-③				40.10	40.05	2.65	45.27	53.86	49.56	6.148		30.859	
No. 11	11-①	0.7	1:2	0:100	40.10	40.05	3.43	51.63	53.30	52.47	7.958	7.177	32.671	32.628
	11-②				40.10	40.05	3.03	52.10	51.38	51.74	7.030		32.217	
	11-③				40.10	40.05	2.82	54.13	51.85	52.99	6.542		32.995	
No. 12	12-①	0.8	1:3	25:75	40.10	40.05	2.57	47.69	48.29	47.99	5.962	6.542	29.882	30.610
	12-②				40.10	40.05	3.36	50.45	49.67	50.06	7.795		31.171	
	12-③				40.10	40.05	2.53	53.39	45.47	49.43	5.870		30.778	
No. 13	13-①	0.8	1:3	50:50	40.10	40.05	3.23	48.98	46.72	47.85	7.494	7.563	29.794	29.944
	13-②				40.10	40.05	3.09	45.64	45.87	45.75	7.169		28.487	
	13-③				40.10	40.05	3.46	52.26	49.08	50.67	8.027		31.550	
No. 14	14-①	0.8	1:3	75:25	40.10	40.05	3.30	51.55	53.83	52.69	7.656	7.030	32.808	32.351
	14-②				40.10	40.05	2.98	54.35	53.34	53.84	6.914		33.524	
	14-③				40.10	40.05	2.81	46.07	52.60	49.34	6.519		30.722	
No. 15	15-①	0.8	1:3	100:0	40.10	40.05	2.75	52.10	54.03	53.06	6.380	6.310	33.039	32.082
	15-②				40.10	40.05	2.82	53.48	47.94	50.71	6.542		31.575	
	15-③				40.10	40.05	2.59	49.79	51.81	50.80	6.009		31.631	

4 Weeks

Test Failure	Specimen		W/C	C:A	S:L	Mass Before Drying (g)	Mass After Drying (g)	Mass Loss (g)	Water Absorption (%)	Avg Water Absorption (%)	Diameter ① (mm)	Diameter ② (mm)	Avg Diameter (mm)	Height (mm)	Volume (cm^3)	Density (g/cm^3)	Avg Density (g/cm^3)	Max Load (kN)	Tensile Strength (N/mm^2)	Avg Tensile Strength (N/mm^2)
Chip/Dent		④				407.4	368.7	38.7	10.496		50.17	50.17	50.170	95.47	188.7	2.16		22.69	3.02	
	No. 1	⑤	0.6	1:1	0:100	409.5	371.7	37.8	10.169	10.955	50.21	50.01	50.110	97.04	191.4	2.14	2.14	27.71	3.63	3.41
		⑥				395.5	352.5	43.0	12.199		50.09	50.08	50.085	94.23	185.6	2.13		26.62	3.59	
		④				401.8	360.6	41.2	11.425		50.21	50.12	50.165	94.65	187.1	2.15		27.98	3.75	
	No. 2	⑤	0.6	1:1	25:75	409.3	355.7	53.6	15.069	13.501	50.16	50.20	50.180	96.50	190.8	2.15	2.14	20.85	2.74	3.31
		⑥				395.5	346.9	48.6	14.010		50.11	50.14	50.125	94.22	185.9	2.13		25.54	3.44	
		④				400.1	340.6	59.5	17.469		50.07	50.14	50.105	98.27	193.8	2.06		26.37	3.41	
	No. 3	⑤	0.6	1:1	50:50	379.4	335.7	43.7	13.018	15.450	50.05	50.03	50.040	95.81	188.4	2.01	2.04	32.18	4.27	4.02
		⑥				392.2	338.5	53.7	15.864		50.04	50.13	50.085	97.68	192.4	2.04		33.73	4.39	
		④				391.3	355.7	35.6	10.008		50.05	50.01	50.030	97.02	190.7	2.05		33.94	4.45	
	No. 4	⑤	0.6	1:1	75:25	380.3	332.5	47.8	14.376	13.994	50.18	50.24	50.210	97.01	192.1	1.98	2.04	32.79	4.29	3.96
		⑥				391.6	333.0	58.6	17.598		50.21	50.16	50.185	94.11	186.2	2.10		23.26	3.14	
		④				388.0	335.5	52.5	15.648		50.13	50.03	50.080	97.30	191.7	2.02		23.52	3.07	
	No. 5	⑤	0.6	1:1	100:0	406.9	354.4	52.5	14.814	15.182	50.18	50.04	50.110	96.47	190.3	2.14	2.05	23.66	3.12	3.13
		⑥				379.2	329.5	49.7	15.083		50.17	50.23	50.200	95.74	189.5	2.00		24.20	3.21	
		④				409.8	367.0	42.8	11.662		50.12	50.19	50.155	94.13	186.0	2.20		32.06	4.32	
	No. 6	⑤	0.7	1:2	0:100	385.6	329.8	55.8	16.919	15.381	50.25	50.09	50.170	96.81	191.4	2.01	2.09	29.25	3.83	4.02
		⑥				396.3	337.1	59.2	17.562		50.00	50.09	50.045	98.03	192.8	2.06		30.23	3.92	
		④				397.1	359.5	37.6	10.459		50.23	50.16	50.195	95.27	188.5	2.11		22.86	3.04	
	No. 7	⑤	0.7	1:2	25:75	392.6	352.5	40.1	11.376	11.147	50.04	50.20	50.120	98.91	195.1	2.01	2.08	27.93	3.59	3.09
		⑥				410.6	367.9	42.7	11.606		50.13	50.22	50.175	97.50	192.8	2.13		20.25	2.64	
		④				385.3	334.8	50.5	15.084		50.16	50.16	50.160	97.08	191.8	2.01		21.53	2.81	
	No. 8	⑤	0.7	1:2	50:50	376.0	339.2	36.8	10.849	12.519	50.13	50.06	50.095	97.28	191.7	1.96	2.03	28.67	3.75	3.31
		⑥				406.2	363.9	42.3	11.624		50.15	50.23	50.190	96.76	191.4	2.12		25.80	3.38	
		④				396.5	339.1	57.4	16.927		50.13	50.20	50.165	97.18	192.1	2.06		23.69	3.09	
	No. 9	⑤	0.7	1:2	75:25	381.9	326.8	55.1	16.860	16.934	50.06	50.11	50.085	98.08	193.2	1.98	2.04	21.57	2.80	2.92
		⑥				398.2	340.3	57.9	17.014		50.10	50.13	50.115	97.55	192.4	2.07		22.06	2.87	
		④				375.7	325.7	50.0	15.352		50.19	50.06	50.125	94.45	186.4	2.02		27.63	3.72	
	No. 10	⑤	0.7	1:2	100:0	388.2	350.4	37.8	10.788	13.220	50.09	50.11	50.100	95.22	187.7	2.07	2.08	29.10	3.88	3.54
		⑥				408.9	360.2	48.7	13.520		50.19	50.07	50.130	96.12	189.7	2.16		22.80	3.01	
		④				377.6	339.7	37.9	11.157		50.18	50.15	50.165	96.26	190.3	1.98		30.70	4.05	
	No. 11	⑤	0.7	1:2	0:100	404.1	361.7	42.4	11.722	11.631	50.20	50.07	50.135	96.91	191.3	2.11	2.05	33.53	4.39	3.74
		⑥				400.9	357.9	43.0	12.015		50.12	50.13	50.125	98.94	195.2	2.05		21.65	2.78	
		④				410.3	359.6	50.7	14.099		50.09	50.21	50.150	96.84	191.3	2.14		23.61	3.09	
	No. 12	⑤	0.8	1:3	25:75	378.9	329.1	49.8	15.132	14.326	50.02	50.01	50.015	95.90	188.4	2.01	2.09	25.94	3.44	3.43
		⑥				394.7	347.0	47.7	13.746		50.21	50.15	50.180	94.59	187.1	2.11		27.97	3.75	
		④				405.4	360.1	45.3	12.580		50.22	50.03	50.125	95.59	188.6	2.15		30.19	4.01	
	No. 13	⑤	0.8	1:3	50:50	384.4	333.2	51.2	15.366	13.144	50.21	50.03	50.120	95.24	187.9	2.05	2.10	24.85	3.31	3.83
		⑥				391.2	350.9	40.3	11.485		50.11	50.14	50.125	95.07	187.6	2.09		31.21	4.17	
		④				402.6	367.1	35.5	9.670		50.11	50.18	50.145	95.99	189.6	2.12		29.24	3.87	
	No. 14	⑤	0.8	1:3	75:25	411.1	351.4	59.7	16.989	14.491	50.15	50.16	50.155	96.30	190.3	2.16	2.13	20.02	2.64	3.37
		⑥				400.2	342.6	57.6	16.813		50.13	50.05	50.090	96.83	190.8	2.10		27.49	3.61	
		④				378.9	339.9	39.0	11.474		50.13	50.09	50.110	95.86	189.0	2.00		30.26	4.01	
	No. 15	⑤	0.8	1:3	100:0	383.2	342.7	40.5	11.818	11.530	50.22	50.22	50.220	95.12	188.4	2.03	2.03	25.55	3.41	3.07
		⑥				401.9	361.1	40.8	11.299		50.10	50.05	50.075	99.05	195.1	2.06		13.94	1.79	

A/C:3/1-W/C:0.8

A/C:2/1-W/C:0.7

A/C:1/1-W/C:0.6

4.6.3 Pictures of tested specimens

All 7 days and 28 days of Representative photographs before testing

All 7 days and 28 days of Representative photographs of tested specimens

Chapter 5
Discussion

This chapter synthesizes the theoretical background established in Chapter 2 with the empirical data presented in Chapter 4. The objective is to provide a comprehensive scientific explanation for the observed behavior of the laterite mortar, specifically addressing the mechanisms that allowed certain mixtures to retain high strength despite the use of porous aggregates, and evaluating the overall feasibility of this material.

5.1 Mechanism of Strength Retention

One of the most significant findings of this study is that the compressive strength of the rich mix (W/C 0.6) did not experience a severe decline, and in some instances even exhibited a slight increase, despite the 100% replacement of hard, dense river sand with porous, weaker laterite sand. Furthermore, the splitting tensile strength remained remarkably robust across all replacement ratios, consistently maintaining a ratio of approximately 1/10th of the compressive strength. These results challenge the conventional assumption that the inclusion of weaker, porous aggregates inevitably leads to a weaker concrete matrix.

This unexpected performance can be primarily attributed to the phenomenon of 'Mechanical Interlocking' occurring at the Interfacial Transition Zone (ITZ). As detailed in Chapter 2, the physical characteristics of the aggregate surface play a decisive role in bond formation. Natural river sand particles, shaped by centuries of aquatic erosion, possess a generally smooth and rounded morphology. While this smooth surface is beneficial for fresh state workability, it offers limited frictional resistance at the microscopic interface with the cement paste. When subjected to stress, the failure path often propagates easily along this relatively weak, smooth boundary.

In stark contrast, the laterite sand used in this study—analogous to crushed red soil—is characterized by a highly irregular, angular shape and a rough, vesicular surface texture. When the cement paste hydrates, particularly in a rich mix where the paste volume is abundant, it physically flows into and infiltrates the surface irregularities and microscopic crevices of the laterite particles.

As the paste hardens, it becomes geometrically 'keyed' into the aggregate, forming a tight, interlocking grip, much like puzzle pieces fitting together. This profound physical bond significantly enhances the frictional resistance to shear and tensile stresses at the ITZ. Consequently, when the hardened mortar is subjected to external loads, the interfacial bond is strong enough that it resists clean separation. Instead of the crack slipping easily around the aggregate (bond failure), the strong mechanical interlock often forces the fracture path to travel directly through the aggregate particles themselves or through the surrounding paste.

This mechanism explains why the splitting tensile strength—a property highly sensitive to bond quality—remained high even when a porous aggregate was utilized. The rough surface texture of the laterite effectively compensated for its lower intrinsic crushing strength by creating a vastly superior aggregate-paste interface.

Fig 5.1: Fracture Surface of Laterite Specimen

5.2 The Filler Effect and Porosity Reduction

A secondary, yet equally critical, mechanism governing the behavior of the laterite mortar is the 'Filler Effect.' As detailed in Chapter 4, the hardened mortar exhibited a counter-intuitive physical property: as the volumetric replacement of porous laterite increased, the overall water absorption of the hardened composite actually decreased. In conventional materials science, the introduction of a highly vesicular and absorptive aggregate is expected to increase the total interconnected porosity of the concrete, thereby increasing water absorption. The reversal of this trend requires a microstructural explanation.

The key to this phenomenon lies in the particle size distribution of the crushed laterite. The Sieve Analysis curve (presented in Section 3.1.3) clearly demonstrated that the laterite sand contains a significantly higher proportion of micro-fines—specifically particles passing the 0.15 mm and 0.3 mm sieves—than the standard river sand. While river sand consists of relatively uniform, coarse grains that leave distinct interstitial gaps when packed together, the crushed laterite possesses a much broader gradation, including substantial volumes of silt and clay-sized rock dust.

During the wet mixing phase, these ultra-fine laterite particles are dispersed homogeneously throughout the cement paste. As the mortar cures and the excess mixing water begins to evaporate, a network of microscopic capillary pores is typically left behind in the paste matrix. It is through these continuous capillary channels that external water usually permeates the concrete. However, in the laterite-modified mixtures, the abundant fine particles physically occupy these interstitial spaces. This phenomenon—where inert fine dust packs into the voids between cement grains and larger aggregates—is academically defined as the physical 'Filler Effect.'

By physically plugging the gaps in the cementitious matrix, the fine laterite dust fundamentally alters the topology of the pore structure. It increases the 'tortuosity' of the capillary network, meaning that any remaining pores become discontinuous, blocked, and highly convoluted. Consequently, even though the laterite aggregate particles themselves contain internal pores, the surrounding cement matrix becomes highly impermeable. External water cannot easily navigate through the blocked capillary channels to reach the aggregate pores. This effectively 'seals' the porous aggregates inside a dense paste shell.

This microstructural densification explains both the physical and mechanical data. It accounts for the unexpected drop in water absorption recorded in Section 4.1.2. Furthermore, it explains why the compressive strength of the rich mixes (W/C 0.6) was not compromised by the weaker aggregate. The Filler Effect increased the solid packing density of the matrix, creating a highly cohesive and continuous load-bearing skeleton that successfully offset the innate structural deficiencies of the porous laterite stone.

5.3 Synergy of Blast Furnace Slag and Laterite Aggregate

The experimental data presented in Chapter 4 clearly identifies Blast Furnace Slag (BF) as the optimal admixture for laterite-based mortar. When 15% of the cement was replaced with BF slag, the 28-day compressive strength of the 100% laterite mix surged to approximately 54 N/mm^2 (at W/C 0.6). This performance dramatically eclipsed both the Plain laterite mix and the Fly Ash mix. To understand why BF slag was uniquely capable of 'rescuing' the structural integrity of the porous laterite mortar, it is necessary to examine the specific chemical and microstructural interactions occurring at the boundary of the aggregate.

5.3.1 Latent Hydraulic Activity and C-S-H Gel Formation

The fundamental weakness of laterite sand is its high porosity. Under normal circumstances, these microscopic voids within the aggregate and at the aggregate-paste interface act as structural flaws, initiating early crack formation under compressive stress. The Plain cement mix lacks the capability to deeply penetrate and permanently seal these microscopic pores.

Blast Furnace Slag, however, possesses 'Latent Hydraulic' properties. When Portland cement hydrates, it releases Calcium Hydroxide (CH) and various alkalis. This highly alkaline environment activates the glassy structure of the slag. Once activated, the fine slag particles react vigorously with water to produce a massive secondary generation of Calcium Silicate Hydrate (C-S-H) gel. This secondary C-S-H gel is physically denser and less permeable than the primary gel produced by Ordinary Portland Cement alone[5].

5.3.2 Densification of the Interfacial Transition Zone (ITZ)

The true synergy between the slag and the laterite occurs at the Interfacial Transition Zone (ITZ). In a plain concrete mix, the ITZ is typically the weakest phase, characterized by high porosity and the accumulation of large, brittle Calcium Hydroxide crystals [12] . Because laterite is a porous, crushed rock, its surface is irregular and covered in open vesicles (pores).

When the BF slag is introduced, its ultra-fine particles migrate into the surface crevices and open pores of the laterite aggregate. As the latent hydraulic reaction proceeds, the dense secondary C-S-H gel precipitates directly inside these aggregate pores and throughout the ITZ. Furthermore, the slag actively consumes the weak Calcium Hydroxide crystals that would normally plague the boundary layer, converting them into additional strong binder [12] .

This chemical process effectively 'welds' the laterite aggregate to the surrounding cement paste. The slag reaction products bridge the gap between the matrix and the stone, filling the remaining voids and transforming a highly porous boundary into a solid, continuous microstructure. By physically plugging the inherent weaknesses of the laterite with high-strength cementitious gel, the slag neutralized the aggregate's primary defect, resulting in the massive surge in macroscopic compressive strength.

5.3.3 Contrast with Fly Ash Performance

The superior performance of the Blast Furnace Slag is further highlighted when contrasted with the Fly Ash (FA) mixtures. The FA mixes demonstrated negligible strength improvements at 28 days. This discrepancy is entirely due to chemical reaction kinetics.

Fly ash is a pozzolanic material, meaning it cannot react directly with water. It must wait for the Portland cement to hydrate and produce sufficient Calcium Hydroxide before its secondary strength-building reaction can begin. This pozzolanic reaction is notoriously slow. At the 28-day testing mark, the majority of the fly ash particles had likely not yet reacted, acting merely as inert physical fillers within the matrix. While the spherical shape of the fly ash may have provided a minor 'filler effect' to aid bending strength, it failed to produce the dense C-S-H gel necessary to chemically weld the porous laterite pores within the required timeframe. Therefore, for short-to-medium-term structural strength, Blast Furnace Slag is the vastly superior admixture for porous aggregate composites.

5.4 Correlation Analysis

To statistically verify the physical mechanisms governing the mechanical performance of the laterite mortar, a series of correlation analyses were conducted. By plotting the experimental data points on scatter graphs and determining the coefficient of determination (R^2), it is possible to identify which material properties dictated the ultimate failure of the composites.

5.4.1 Density vs. Compressive Strength

In conventional concrete technology, hardened density is widely regarded as a primary predictor of compressive strength. The general rule asserts that heavier, denser concrete contains fewer air voids and therefore exhibits higher load-bearing capacity. However, Figure 5.3 reveals a highly irregular and significant finding regarding the laterite mortar.

The scatter plot of Hardened Density versus Compressive Strength resulted in an almost perfectly flat trendline, with a correlation coefficient near zero ($R^2 \approx 0.0041$). This lack of correlation is a critical discovery. The near-zero R^2 value indicates that hardened density showed little linear relationship with compressive strength within the present dataset. This suggests that bulk density alone was not a reliable predictor of compressive strength for the mixtures tested. By contrast, water absorption showed a moderate negative correlation with compressive strength, indicating that porosity-related effects were more influential than density alone. Even as the density of the mortar decreased (due to minor air entrapment from the sticky, fines-rich paste), the compressive strength remained high and stable.

This statistical flatness confirms the physical theories proposed earlier in this chapter: the structural integrity of the laterite mortar is driven by the 'Mechanical Interlocking' of the rough aggregate surfaces and the densification of the ITZ, rather than sheer mass. This indicates that laterite can successfully be utilized to produce a semi-lightweight mortar without sacrificing necessary structural strength, offering distinct advantages for reducing dead loads in building design.

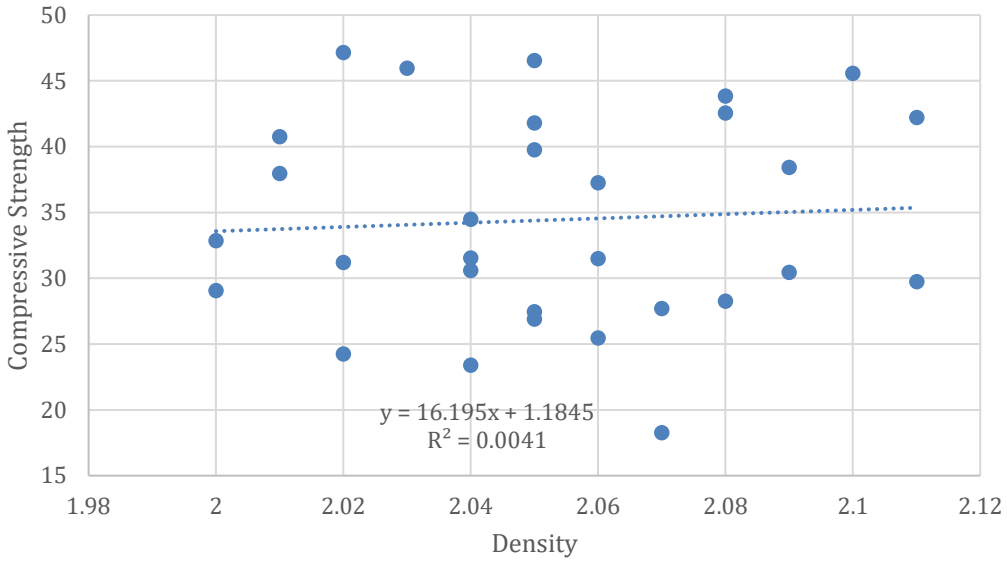

Fig 5.3: Correlation between Density and Compressive Strength

5.4.2 Water Absorption vs. Compressive Strength

While bulk density failed to predict mechanical performance, water absorption proved to be a highly reliable indicator. Water absorption is a direct macroscopic measurement of the interconnected capillary porosity within the hardened matrix. Figure 5.4 illustrates the relationship between Water Absorption and Compressive Strength.

The scatter plot displays a clear and significant negative correlation ($R^2 = 0.5989$). As the percentage of water absorption increased, the compressive strength of the mortar predictably and linearly decreased. This statistically confirms that porosity is the primary 'enemy' of strength in laterite-based composites. The interconnected voids act as stress concentrators where micro-cracks originate and easily propagate under compressive loading.

This strong negative correlation also validates the success of the 'Filler Effect' and the Blast Furnace Slag admixtures. The data points representing the highest compressive strengths all cluster at the lowest water absorption values. By physically blocking the pores with fine

laterite dust and chemically sealing them with secondary C-S-H gel from the slag, the porosity was minimized, directly translating into the massive strength gains observed.

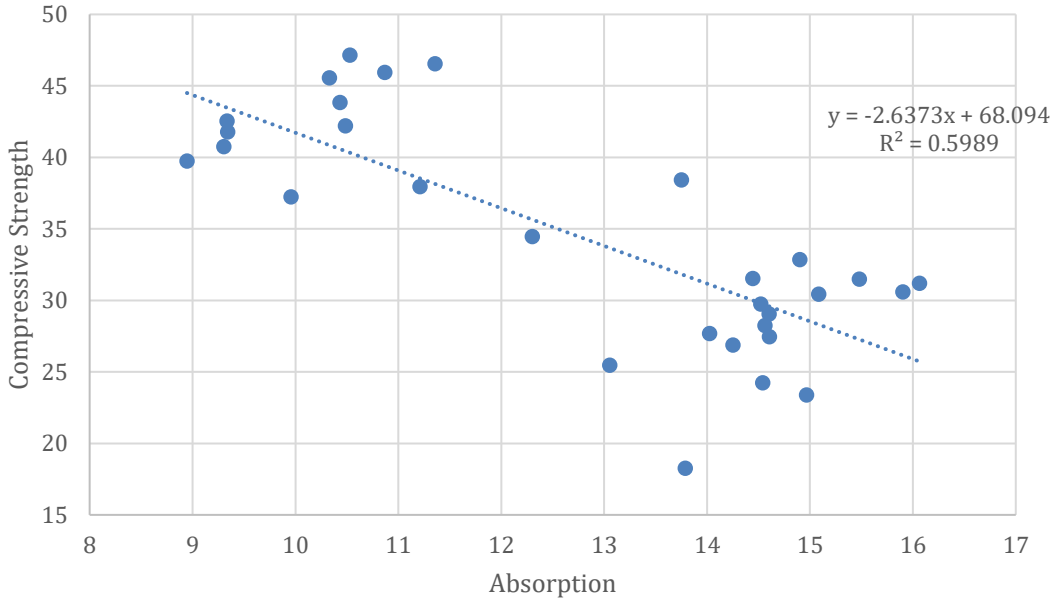

Fig 5.4: Correlation between Water Absorption and Compressive Strength

5.4.3 Inter-relationship of Mechanical Strengths

Finally, the relationship between compressive strength and the tensile properties (bending and splitting tensile strength) was analyzed to evaluate the overall structural integrity and ductility of the composite. A common concern when utilizing porous or unconventional aggregates is that the resulting concrete may become overly brittle, leading to sudden, catastrophic failure under tensile stress.

Figure 5.5 and Figure 5.6 present the correlations between Compressive Strength and Bending/Tensile Strength, respectively. Both graphs exhibit distinct, positive linear trends. The bending strength showed a particularly strong correlation ($R^2 = 0.83$), while the splitting tensile strength correlation was moderate but clear ($R^2 = 0.55$).

Crucially, the upward slope of these trendlines demonstrates that as the compressive strength increased, the tensile and flexural capacities increased proportionally. The splitting tensile strength maintained a standard, healthy ratio of approximately 1/10th of the compressive

strength across the various mixes. This proves that the inclusion of the porous laterite aggregate did not induce dangerous brittleness or compromise the fundamental mechanics of the mortar. The strong correlation reinforces the conclusion that the rough surface texture of the laterite provided a superior, highly frictional mechanical bond with the cement paste, preserving the structural ductility of the composite.

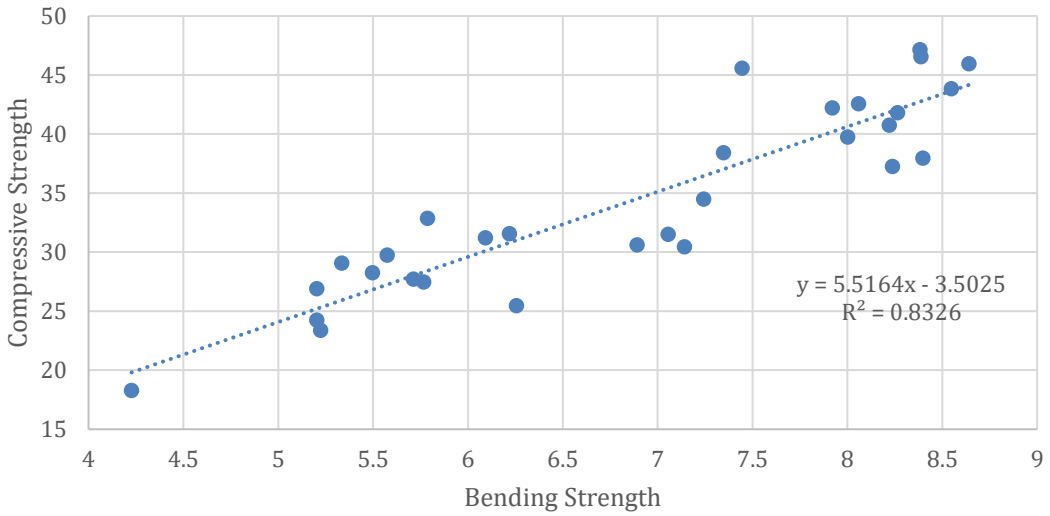

Fig 5.5: Correlation between Compressive and Bending Strength

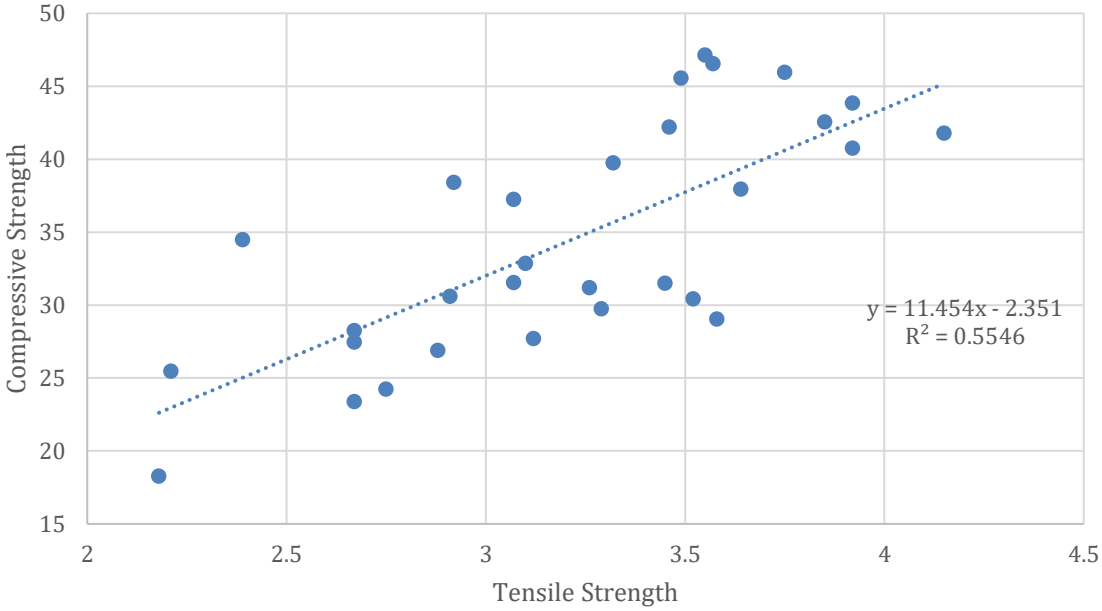

Fig 5.6: Correlation between Compressive and Tensile Strength

Chapter 6

Conclusion

6.1 Summary of Findings

This research was conducted to address the critical environmental and economic crisis caused by the over-extraction of river sand in Southeast Asia. By utilizing Japanese 'En-tout-cas' (red clay soil) as an experimental simulation for Cambodian Laterite, this study systematically evaluated the feasibility, physical properties, and mechanical performance of laterite-based mortar. Based on the comprehensive experimental data and correlation analyses, the following primary conclusions are drawn:

- **1. Feasibility of 100% Replacement in Rich Mixes:** The complete (100%) substitution of natural river sand with laterite sand is highly viable, provided the cement paste volume is sufficient. At a Water-Cement ratio of 0.6, the laterite mortar maintained excellent structural stability, achieving compressive strengths in excess of 30 N/mm². However, the application is limited in lean mixes (W/C 0.8), where the lack of cement paste causes a severe drop in strength.
- **2. Porosity Reduction via the 'Filler Effect':** Contrary to the assumption that using a porous aggregate increases the permeability of the concrete, the hardened water absorption actually decreased as laterite content increased. This is attributed to the 'Filler Effect.' The high volume of fine particles (dust and silt) inherent in the crushed laterite effectively plugged the microscopic capillary voids in the cement matrix, increasing tortuosity and preventing water ingress.
- **3. High Tensile Strength through 'Mechanical Interlocking':** The splitting tensile and bending strengths of the laterite mortar remained robust, maintaining a standard ratio of approximately 1/10th of the compressive strength. This proves that the material does not suffer from extreme brittleness. The rough, highly angular surface texture of the crushed laterite aggregate provided a superior physical grip—or 'Mechanical Interlocking'—with the cement paste, resulting in a stronger Interfacial Transition Zone (ITZ) than what is typically achieved with smooth, rounded river sand.
- **4. The Ultimate Modifier: Blast Furnace Slag:** The addition of mineral admixtures revealed that Blast Furnace Slag (15% cement replacement) is the ultimate modifier for laterite mortar. The latent hydraulic reaction of the slag chemically densified the pore structure and fortified the aggregate-paste boundary [5]. This synergistic effect resulted in

a massive surge in mechanical capacity, driving the compressive strength to approximately 54 N/mm² at 28 days, far outperforming both the Plain and Fly Ash mixtures.

6.2 Recommendations and Future Works

The findings of this study confirm that Laterite Sand is not merely a waste material, but a highly capable construction aggregate when engineered correctly. To translate these laboratory findings into real-world applications, the following recommendations are proposed:

Practical Application in Cambodia: Given the impressive mechanical strength and slightly lower bulk density achieved by the Slag-modified laterite mix (W/C 0.6), Based on the present laboratory results, the slag-modified laterite mortar shows promising potential for non-structural and low-risk construction applications in Cambodia. However, field validation, durability assessment, and testing using actual Cambodian laterite sources are still required before broader practical adoption can be recommended. It is an ideal, low-cost, and eco-friendly alternative for manufacturing Concrete Masonry Units (CMUs), interlocking pavement blocks, and low-to-mid-rise residential wall panels. Adopting this mix design would significantly alleviate the environmental strain currently placed on the Mekong River ecosystem.

Future Research on Durability: While the 28-day mechanical properties have been proven to be exceptional, future studies must evaluate the long-term durability of the laterite mortar. It is highly recommended to conduct accelerated weathering tests, specifically focusing on drying shrinkage, wetting-drying cycles (to simulate the tropical monsoon climate of Southeast Asia), and freeze-thaw resistance (if applied in colder regions like Japan). Furthermore, testing this optimized mix design using raw, unrefined laterite soil directly excavated from Cambodian provinces (such as Siem Reap or Kampong Cham) should be the next critical step toward full-scale industrial implementation.

References

[1] UNEP (United Nations Environment Programme). (2022, April 26). Sand and Sustainability: 10 Strategic Recommendations to Avert a Crisis. UNEP.
https://www.unep.org/resources/report/sand-and-sustainability-10-strategic-recommendations-avert-crisis

[2] BBC News. (2017, July 13). Cambodia bans sand exports permanently.
https://www.bbc.co.uk/news/business-40590695

[3] Encyclopaedia Britannica. (n.d.). Laterite. Accessed 2026-03-03.
https://www.britannica.com/science/laterite

[4] Cuesta, A., Zea-García, J. D., Londono-Zuluaga, D., De la Torre, A. G., Santacruz, I., Vallcorba, O., Dapiaggi, M., Sanfélix, S. G., & Aranda, M. A. G. (2018). Multiscale understanding of tricalcium silicate hydration reactions. Scientific Reports, 8, 8544.
https://doi.org/10.1038/s41598-018-26943-y

[5] Choi, S., & Pyo, S. (2020). Fresh and Hardened Properties of Portland Cement–Slag Concrete Activated Using the By-Product of the Liquid Crystal Display Manufacturing Process. Materials, 13(19), 4354.
https://doi.org/10.3390/ma13194354

[6] Japanese Industrial Standards (JIS). (2018). JIS A 1108:2018 — Method of test for compressive strength of concrete. ANSI Webstore.
https://webstore.ansi.org/standards/jis/jis11082018

[7] Japanese Industrial Standards (JIS). (2018). JIS A 1113:2018 — Method of test for splitting tensile strength of concrete. ANSI Webstore.
https://webstore.ansi.org/standards/jis/jis11132018

[8] Neville, A. M. (2011). Properties of Concrete (5th ed.). Pearson Education.
https://www.pearson.com/en-gb/subject-catalog/p/properties-of-concrete-properties-of-concrete/P200000005116/9780273755807

[9] VnExpress International. (2023, September 3). Illegal sand mining crackdown cuts construction material supply.
https://e.vnexpress.net/news/news/environment/illegal-sand-mining-crackdown-cuts-construction-material-supply-4647079.html

[10] Bhandari, S. R. (2023, March 14). More than 100 million tons of sand mined from Lower Mekong, experts say. Radio Free Asia.
https://www.rfa.org/english/news/environment/mekong-sand-03142023064512.html

[11]Flynn, G., & Srey, V. (2022, August 29). Mining the Mekong: Land and livelihoods lost to Cambodia's thirst for sand. Pulitzer Center.
https://pulitzercenter.org/stories/mining-mekong-land-and-livelihoods-lost-cambodias-thirst-sand

[12] Gao, J. M., Qian, C. X., Liu, H. F., Wang, B., & Li, L. (2005). ITZ microstructure of concrete containing GGBS. Cement and Concrete Research, 35(7), 1299–1304.
https://doi.org/10.1016/j.cemconres.2004.06.042